CALIFORNIA ENERGY COMMISSION

CALIFORNIA NATURAL RESOURCES AGENCY

ENERGY RESEARCH AND DEVELOPMENT DIVISION

FINAL PROJECT REPORT

Improving Hydrologic and Energy Demand Forecasts for Hydropower Operations with Climate Change

June 2024 | CEC-500-2024-059

PREPARED BY:

Bita Analui and Saroosh Sarooshian
Center for Hydrometeorology and Remote Sensing, The Henry Samueli School of Engineering
University of California Irvine
Primary Authors

Joe O'Hagan
Project Manager
California Energy Commission

Agreement Number: 300-15-005

Alex Horangic
Branch Manager
SUSTAINABILITY AND RESILIENCE BRANCH

Jonah Steinbuck, Ph.D.
Director
ENERGY RESEARCH AND DEVELOPMENT DIVISION

Drew Bohan
Executive Director

ACKNOWLEDGEMENTS

The principal investigator's research group gratefully acknowledges the funding opportunity provided by the Electric Program Investment Charge (EPIC) program, California Energy Commission, without which these research activities would not be possible.

The team is also thankful for the constant supports and valuable inputs from Commission Agreement Leads Mr. Guido Franco, Dr. Katharina Gerber, and Mr. Joe O'Hagan during the course and close-out of the project.

PREFACE

The California Energy Commission's (CEC) Energy Research and Development Division supports energy research and development programs to spur innovation in energy efficiency, renewable energy and advanced clean generation, energy-related environmental protection, energy transmission, and distribution and transportation.

In 2012, the Electric Program Investment Charge (EPIC) was established by the California Public Utilities Commission to fund public investments in research to create and advance new energy solutions, foster regional innovation, and bring ideas from the lab to the marketplace. The EPIC Program is funded by California utility customers under the auspices of the California Public Utilities Commission. The CEC and the state's three largest investor-owned utilities—Pacific Gas and Electric Company, San Diego Gas and Electric Company, and Southern California Edison Company—were selected to administer the EPIC funds and advance novel technologies, tools, and strategies that provide benefits to their electric ratepayers.

The CEC is committed to ensuring public participation in its research and development programs that promote greater reliability, lower costs, and increase safety for the California electric ratepayer and include:

- Providing societal benefits.
- Reducing greenhouse gas emission in the electricity sector at the lowest possible cost.
- Supporting California's loading order to meet energy needs first with energy efficiency and demand response, next with renewable energy (distributed generation and utility scale), and finally with clean, conventional electricity supply.
- Supporting low-emission vehicles and transportation.
- Providing economic development.
- Using ratepayer funds efficiently.

For more information about the Energy Research and Development Division, please visit the CEC's research website (www.energy.ca.gov/research/) or contact the Energy Research and Development Division at ERDD@energy.ca.gov.

ABSTRACT

Hydropower is an integral part of supplying clean electricity to the state's electric grid. Besides providing baseload generation, hydropower is increasingly used to mediate load variability in the electrical grid due to the intermittent nature of wind and solar generation. Given the increasing potential of hydropower to meet energy demands, especially in the modernized electric grid, accurate and timely precipitation estimates are critical for optimizing hydropower scheduling. Despite having high-resolution satellite information, precipitation estimation for determining hydrologic flows from remotely sensed data suffer from methodological limitations. State-of-the-art deep learning algorithms, renowned for their skill in learning accurate patterns within large and complex datasets, appear well suited for precipitation estimation.

Advanced machine and deep learning mechanisms were developed to improve the accuracy of precipitation forecasts of an existing real-time Precipitation Estimation from Remotely Sensed Information using Artificial Neural Networks (PERSIANN) algorithm. The precipitation estimates delivered by the improved PERSIANN were used as the main input to a hydrological model to generate daily streamflow information.

Improving the accuracy and time resolution of streamflow data contributes to an increase in confidence and higher efficiency of hydropower scheduling decisions generated by both the reservoir and the hydropower dispatch models used by facility operators. Hydropower release decision making relies on multisource information such as climate conditions, downstream water quality, inflow and storage, regulation, and engineering constraints. To improve this decision making, this study developed meta-heuristic generalized reservoir releases and simulation algorithms for optimizing hydropower operations. A case study of a major operational hydropower facility serving California was presented to demonstrate the improvement of the streamflow simulation and forecast accuracy, based on improved precipitation estimates in PERSIANN products.

Keywords: Precipitation Estimation, Precipitation Forecast, Machine Learning, Artificial Neural Network, Hydropower Operations, Optimization, Precipitation Estimation from Remotely Sensed Information using Artificial Neural Networks (PERSIANN)

Please use the following citation for this report:

Analui, Bita and Soroosh Sorooshian. 2024. Improving Hydrologic and Energy Demand Forecasts for Hydropower Operations with Climate Change. California Energy Commission. Publication Number: CEC-500-2024-059.

TABLE OF CONTENTS

LIST OF FIGURES

LIST OF TABLES

Executive Summary

California's hydropower is an integral part of supplying clean electricity to the state's electric grid. Hydropower provides baseload generation and is able to adjust production, offering load-following services that can help meet unexpected spikes (or troughs) in energy demand, without disruption to the grid. This role for hydropower is becoming increasingly critical as it alleviates the intermittent nature of wind and solar generation as California strives to achieve its ambitious mandate of 100 percent renewable energy and zero-carbon resources supply by 2045.

Hydropower's role in meeting load variability in the electrical grid is particularly sensitive to accurate and timely precipitation and inflow forecasts. Precipitation and inflow forecasts are especially important for run-of-river hydropower plants (hydropower generation that uses the natural flow rate of water to generate power) and hydropower scheduling (the scheduling of water releases from a hydropower facility). Reservoirs play an essential role in providing resilience against flood and drought, and additionally supply a wide range of services including water supply, hydropower electricity, recreation, and ecosystem protection. There is therefore an important need to properly address, through reservoir modelling, these various services, while respecting underlying regulations. Although reservoir modelling and optimal reservoir operations have been well studied, there is still vast research potential to address the credibility of forecasts used for reservoir modelling.

The development of Earth-observing satellites that measure precipitation have overcome many of the limitations of land- and radar-based precipitation measurements. Satellite-based precipitation estimates provide high temporal and spatial resolution; but precipitation estimation for determining hydrologic flows from remotely sensed data still suffers from methodological limitations. State-of-the-art deep learning algorithms, renowned for their accuracy in producing accurate patterns within large and complex datasets, appear well suited to the task of precipitation estimation given the ample amount of available high-resolution satellite data.

Project Purpose

To support more accurate and optimal hydropower scheduling for utilities serving California, the purpose of this research was to:

1. Enhance short-term precipitation streamflow forecasts by developing an operating module for an existing near real time Precipitation Estimation from Remotely Sensed Information using Artificial Neural Networks (PERSIANN) product that has demonstrated advantages over other quantitative precipitation estimation algorithms over the Western continental United States.
2. Provide more accurate assessments of hydropower generation capabilities by developing a generalized reservoir release and hydropower production model for major reservoirs in California.

Project Approach and Results

The focus of this project by researchers from the University of California, Irvine's, Center for Hydrometeorology and Remote Sensing was to develop advanced machine and deep learning mechanisms to improve the accuracy of precipitation forecasts of an existing near real-time PERSIANN model. The precipitation estimates delivered by the improved PERSIANN were used as the main inputs to a hydrological model that generates daily streamflow information.

Improved accuracy and time resolution of streamflow data contributed to increased confidence in and higher efficiency of hydropower scheduling decisions generated by the reservoir and hydropower dispatch models used by hydropower facility operators. Precipitation measurements with high space/time resolution are vital inputs for hydrometeorological and water resources studies, weather, climate, and hydrological forecasting. Moreover, highly precise real-time precipitation estimations are pivotal for monitoring and managing catastrophic hydroclimate events such as flash floods, which frequently transpire rapidly after extreme rainfall. To this end, a model and nine algorithms were developed.

1. The PERSIANN Dynamic Infrared Rain-Rate Model estimated precipitation rates from satellite infrared radiation imagery, which offered notable advantages over current algorithms for rainfall estimation, especially over the Western Contiguous United States.
2. Six advanced *machine learning and neural network* algorithms improved the PERSIANN family and delivered precipitation estimation and short-term forecasts more accurately.
3. Three generalized reservoir-release and hydropower-optimization algorithms leveraged data-driven and meta-heuristic approaches, which analyzed streamflow simulation improvements and forecast accuracy based on improved precipitation estimates. Applications in California assisted hydropower management in a major operational facility in California.

These three components, the improved and bias corrected data, the short-term precipitation forecast module, and reservoir optimization algorithms, together represent a fully connected modeling approach.

Knowledge Transfer

This research has been shared in presentations through more than 30 invited and accepted talks at different conferences and academic institutions such as the multiple papers presented at the 2019 American Geoscience Union Fall Meeting. In addition, the knowledge gained, experimental results, and lessons learned were reflected in more than 16 peer-reviewed journal publications, five PhD theses, and nine developed algorithms.

Benefits to California

Using the developed components of this research (in the form of the PERSIANN Dynamic Infrared Rain-Rate Model, a real-time global high-resolution satellite precipitation estimation product), the advanced machine learning algorithms to improve precipitation estimation and forecasts, and the reservoir modeling/optimization algorithms, would enable more efficient management of clean energy resources in California and lead to improved resilience of water and energy systems in the face of climate change impacts. Advancing these algorithms and model for hydropower scheduling and prediction will also facilitate electricity exchanges in the power markets, reduce consumption of non-renewable energy sources, and increase the reliability of renewable resource energy generation.

CHAPTER 1: Introduction

In this chapter, the foundations upon which the project approaches are built are presented. Since this research investigated, analyzed, and improved the accuracy of the Precipitation Estimation from Remotely Sensed Information using Artificial Neural Networks (PERSIANN) products at different weather and climate scales, the PERSIANN algorithm is introduced. As its name indicates, PERSIANN uses a machine learning technique to determine the relationship between remotely sensed cloud-top temperatures (measured by long-wave infrared [IR] sensors on geosynchronous equatorial orbit satellites) and rainfall rates, with bias correction from passive microwave readings measured by low Earth-orbiting satellites. Gridded precipitation products like PERSIANN are useful in the research, community, and private sectors for hydrologic modeling, flood, and drought predictions, water resource management, and urban planning. The quasi-global scope of these satellite-based precipitation products makes them practical for quantifying rainfall measurements over space and time, notably in regions lacking large-scale systems of precipitation gauges or a radar network (for example, over the oceans).

Accurate observations of the global distribution of precipitation are required for monitoring the variability of weather and climate and are crucial to the development of a proper understanding of the hydrologic cycle as it passes through oceans, land, and the atmosphere. For hundreds of years, rainfall has been measured by the conventional method of rain gauges, but this method facilitates only a relatively sparse sampling of rainfall, primarily over land. The use of ground-based radar now enables the measurement of rainfall over relatively large areas, but the coverage is still essentially limited to land surfaces and coastal regions. With the current rapid growth in satellite remote-sensing technology, the global distribution of rainfall, even over the oceans, can be routinely monitored (Hsu et al., 1997). At the University of Arizona, PERSIANN was developed by Hsu (1997) to extract and combine various sources of information including, for example, infrared and microwave satellite imagery, rain gauge and ground-based radar data, and ground-surface topographic information to estimate rainfall.

The current operational PERSIANN system at the University of California, Irvine[1], uses neural network function classification and approximation procedures to compute estimated rainfall rates at 0.25° x 0.25° pixel (about 27.75 km x 27.5 km) of the infrared brightness temperature image provided by geostationary satellites. An adaptive training feature facilitates updating of the network parameters whenever independent estimates of rainfall are available. The PERSIANN algorithm is an effective and efficient approach in retrieving rainfall using cloud-top brightness temperature (CTBT) data in quasi-global coverage (60°N to 60°S). Two major stages in PERSIANN are involved in processing a satellite image into surface rainfall rates. The algorithm first extracts and classifies local texture features from the long-wave infrared image of geostationary satellites to several texture patterns, then associates those classified cloud

[1] http://chrsdata.eng.uci.edu/

texture patterns to surface rainfall rates. Figure 1 shows the precipitation generation flow from the PERSIANN algorithm.

Behrangi (2009) and AghaKouchak (2011) have shown that the PERSIANN algorithm is a suitable candidate for estimating precipitation from short-term CTBT forecasts due to the capability of the model in estimating high-resolution half-hourly rainfall rate maps (where other precipitation retrieval models have coarser temporal resolution).

Figure 1: The PERSIANN System

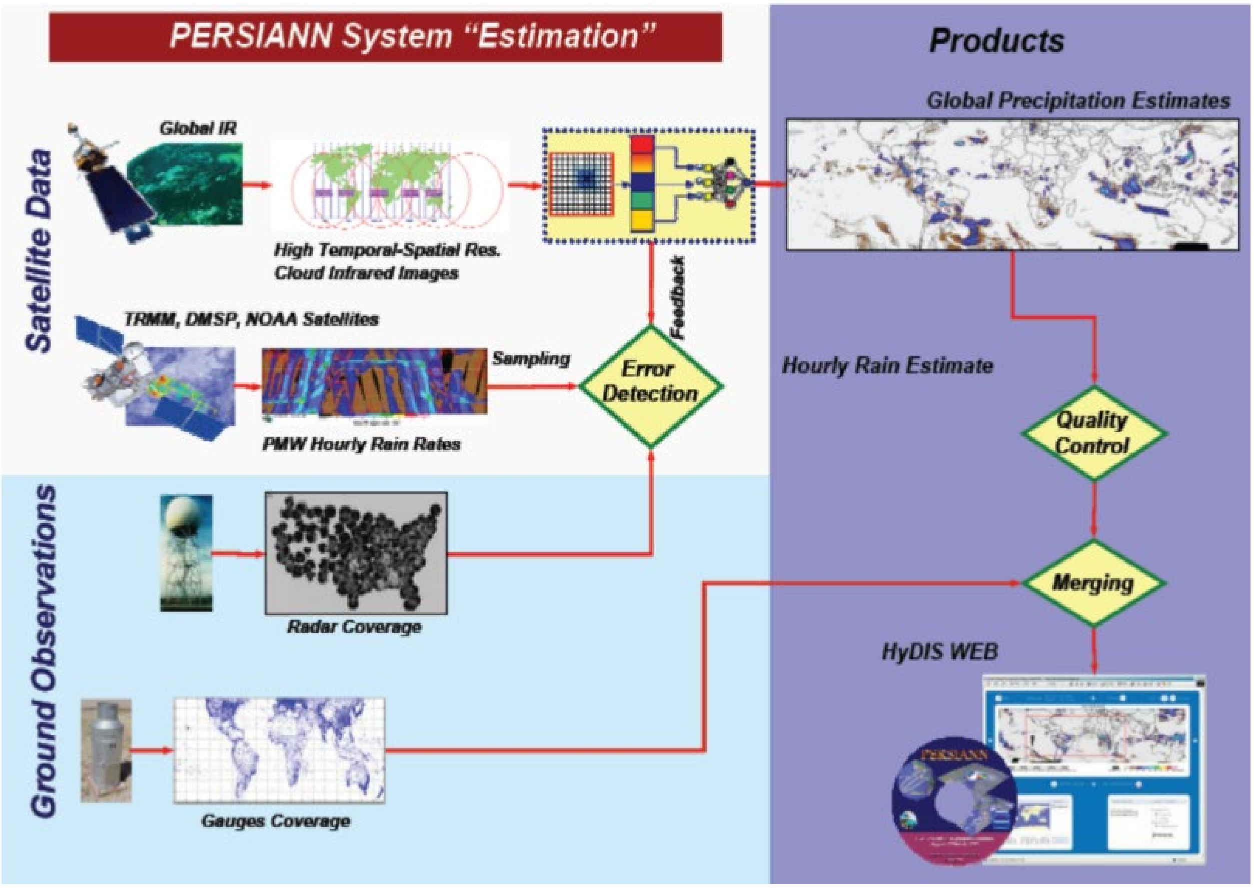

Operational implementation of the PERSIANN system produces and distributes near-real-time global precipitation products at 0.25°(27.5km) hourly resolution.

Source: Sorooshian et al., 2007

CHAPTER 2: Project Approach and Results

Over the past two decades, a wide range of studies has incorporated PERSIANN products. Currently, PERSIANN offers several precipitation products based on different algorithms available at various spatial and temporal scales. The following discussion highlights the research carried out in this project and identifies new PERSIANN products, enhancements, and case studies.

PERSIANN Dynamic Infrared-Rain Rate Model (PDIR) for High-Resolution, Real-Time Satellite Precipitation Estimation

(Nguyen et al., 2020)

Previous research (Hsu et al., 1997) suggests that one of the main reasons for substantial errors in hydrologic forecasting is a lack of quality data on temporal and spatial variations of historical precipitation. Building on the foundations of the PERSIANN family, a new algorithm to estimate the precipitation rate from satellite infrared radiation imagery was developed. This offers notable advantages over current algorithms for rainfall estimation, especially over the western portion of the contiguous United States (CONUS).

In the PERSIANN cloud classification system (CCS), clouds that are identical in shape, size, temperature distribution, and all other defining characteristics (except spatial location), have identical rain rates (RR). The new algorithm, the PERSIANN Dynamic Infrared-Rain Rate Model (PDIR-Now), advances the framework of the PERSIANN-CCS system by:

1. Improving the capture of warm precipitation by adapting higher temperature thresholds and introducing gradient filtering and applying morphological filters to improve watershed methods of segmentation.
2. Expanding the cloud classification system to include monthly sets of cloud types and improving the algorithm's ability to distinguish between different rainfall regimes.
3. Improving the skill of CTBT-RR curves with the National Oceanic and Atmospheric Administration's (NOAA) passive microwave dataset.
4. Using gridded climatology data from WorldClim (version 2) and the PERSIANN climate data record (CDR) to create a dynamical RR curve model optimized by a shuffled complex evolution algorithm.

Figure 2 shows that drier climates, such as in the Mojave Desert, cause a leftward shift in the CTBT-RR relationships, which results in lower precipitation rates than at identical temperatures in moderately wet regions such as the California Central Coast, while wetter climates such as in the Klamath National Forest cause a rightward shift, which in turn causes an increase in estimated precipitation rates for identical temperatures.

Figure 2: The Dynamic CTBT (Tb)-Rain Rate (RR) Model

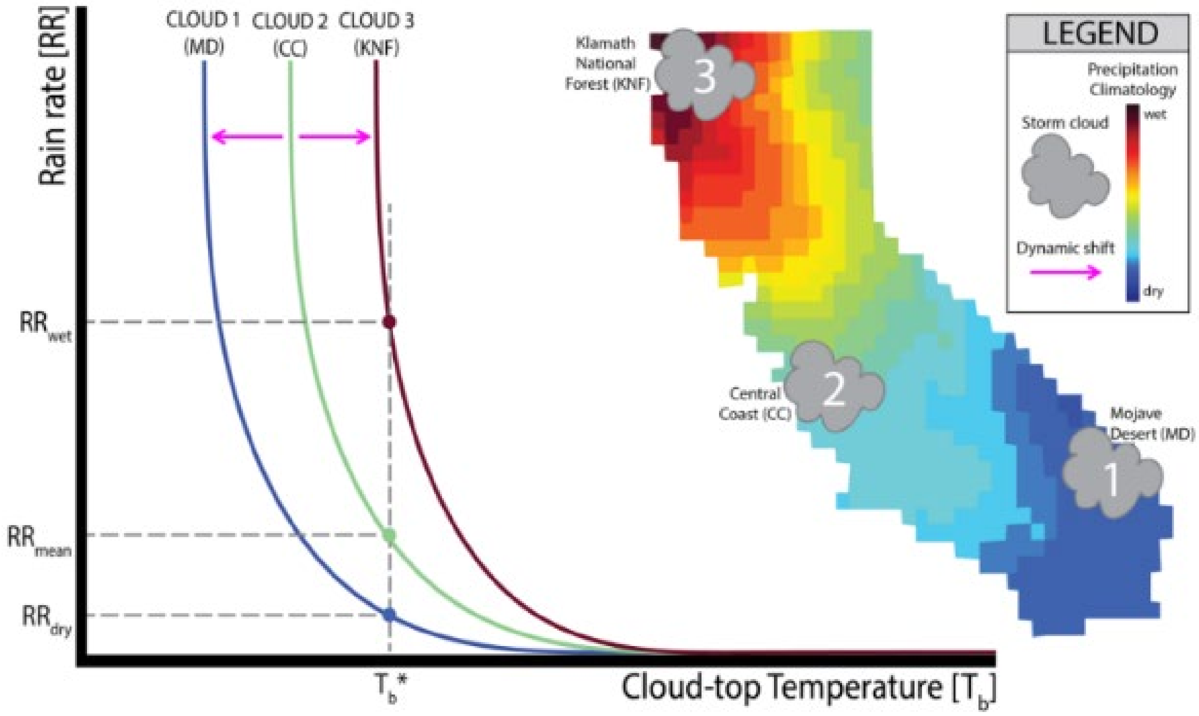

In PERSIANN-CCS, clouds that are identical in shape, size, temperature distribution, and all other defining characteristics (but spatial location) have completely identical RR readings.

Source: Nguyen et al., 2020

In the PDIR-Now workflow, brightness temperature IR is read as the sole input by the fully trained PDIR-Now algorithm. After cloud patches are extracted with the assistance of the modified watershed technique, a vector of 17 characteristics is pulled from each cloud patch. The vector is fed into the month's self-organizing feature map of cloud types, which returns the most likely cloud type given the extracted characteristics. Each cloud type has a characteristic Tb-RR relationship that is dynamically shifted according to pixel climatology and cloud type before PDIR-Now pulls the final RR estimate. A flowchart of the PDIR-Now steps, from input to output, is shown in Figure 3.

PDIR-Now estimates were validated over the western contiguous United States at annual and daily levels during the validation period of 2008-13. In addition, short-time-scale validation were performed for two specific extreme atmospheric river (AR) events, as ARs are intimately related to water resources and natural hazards in Pacific Ocean coastal states.

Figure 3: PDIR-Now Workflow From Input to Output

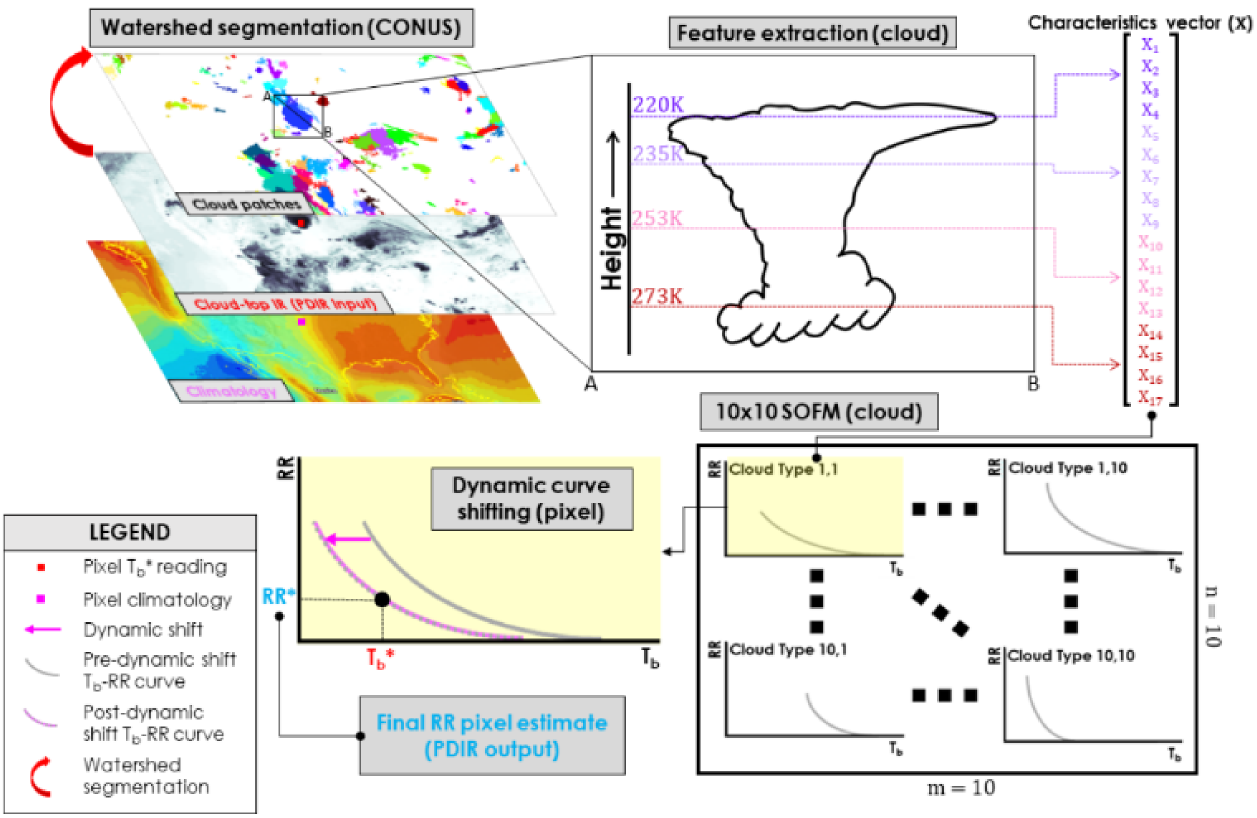

SOFM = self-organizing feature map
Source: Nguyen et al., 2019

Atmospheric River Event Over California, March 20 to 25, 2018

The 2018 AR event of March 20 to 25, belonged to a specific category of ARs known as the Pineapple Express. These ARs originate over Hawaii and move from the equatorial Pacific toward the West Coast of the United States. During this period, rainfall totals of 230 millimeters (mm) were recorded in some regions, during the first day alone. Figure 4 shows the rainfall accumulation during the six-day period of the storm. The observed (Stage IV) rainfall spatial pattern consisted of a band of heavy rainfall along the Sierra Nevada and disconnected bands of heavy rainfall along the California coast. Although all satellite-based products — the Integrated Multi-Satellite Retrievals Climate Prediction Center MORPHing technique (CMORPH), tropical rainfall measuring mission (TRMM), and PERSIANN-CCS — estimate heavy rainfall during the storm period, PDIR-Now is the only product that mimics observed spatial rainfall patterns *apart from* underestimation over the northern coast of California. In addition to better spatial patterns, PDIR-Now estimates more accurate rainfall amounts than other products with a correlation coefficient (CORR) of 0.74 and root mean square error (RMSE) of 41 mm; PDIR-Now is superior to Stage II for detecting heavy storm rainfall in terms of both spatial pattern and volume. In addition to the metrics just discussed, PDIR-Now has a relative bias (rBIAS) of −0.40, which is superior to Stage II's CORR, RMSE, and rBIAS values of 0.63, 57.87 mm, and −0.73. This shows that PDIR-Now has potential benefits in storm monitoring, designing early warning systems, and disaster management planning for heavy storms associated with ARs over the western coast of the United States.

The research team observed that PDIR-Now, a remotely sensed precipitation algorithm that solely uses IR as input data, was comparable (or of greater relative skill) to passive microwave, radar, and other IR-based products for both annual accumulations and short-term extreme weather events. Furthermore, PDIR-Now accurately mimicked the observed spatial patterns of rainfall over the study region, notably high rainfall amounts over the Cascade Range and the Sierra Nevada. PDIR-Now's noteworthy performance in capturing the western states' rainfall — especially with high intensities and over mountainous regions — suggests a level of success in adapting to the challenges of differing rainfall regimes intrinsic to the area.

PDIR-Now contains the spatiotemporal richness and near instantaneous availability (15 minutes to one hour) required for rapid hazard response, while showing the potential for enough skill to be useful for hydrologic and water resources applications; the latter has been a major weakness of IR-based algorithms to date. However, future analysis into PDIR-Now's skill specific to each rainfall regime must be performed before final concrete conclusions can be made.

Figure 4: Rainfall During March 20 to 25, 2018

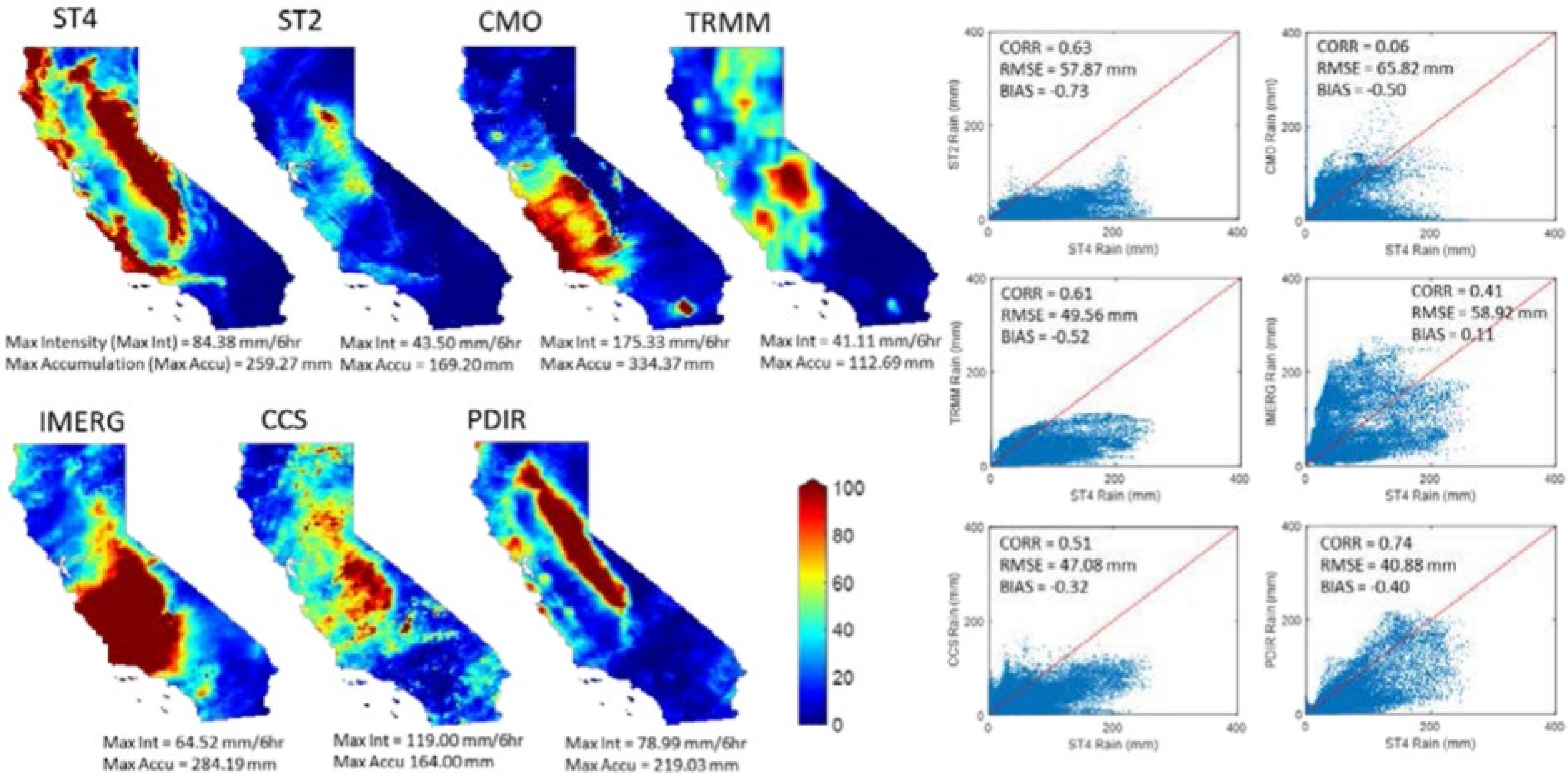

An extreme AR event over California. Six-hourly observations from ground measurements: Stage IV and the near real-time Stage II, satellite-based measurements: CMORPH, TRMM, PERSIANN-CCS (CCS) and PDIR-Now.

Source: Nguyen et al., 2019

Developing Precipitation Estimation and Forecast Modules — Machine Learning and Artificial Neural Network Models

In this section, a range of advance precipitation forecasts and estimation algorithms (based on machine learning and neural network models) is presented.

Precipitation Forecast

Prediction Skill for the West Coast United States: From Short to Extended Ranges

(Pan et. al., 2019a)

Precipitation variability significantly influences the heavily populated West Coast of the United States, raising the need for reliable predictions. The team investigated the region's short-to-extended-range precipitation prediction skill using the hindcast database of the World Meteorological Organization's Sub-seasonal-to-Seasonal (S2S) Prediction Project (WMO, 2018). The prediction skill/lead time relationship was also evaluated, using both deterministic and probabilistic skill scores. The study area was restricted to the heavily populated coastal region of the Western United States, which included California, Western Oregon, and Western Washington. Figure 5 shows the geographic map of the West Coast in sub-figure (a). The elevation data are provided by United States Geological Survey (Gesch, 2002). The four subdivisions, namely Southern California, Northern California, Western Oregon, and Western Washington states, are outlined with colored polygons. Geo-position of the study area in a larger scale is shown in sub-figure (b). The monthly mean precipitation rate for the four subdivisions, based on the Climate Prediction Center (CPC) precipitation dataset and the boreal winter (October to March) precipitation ratio, is labeled in sub-figure (c).

Figure 5: The Study Area

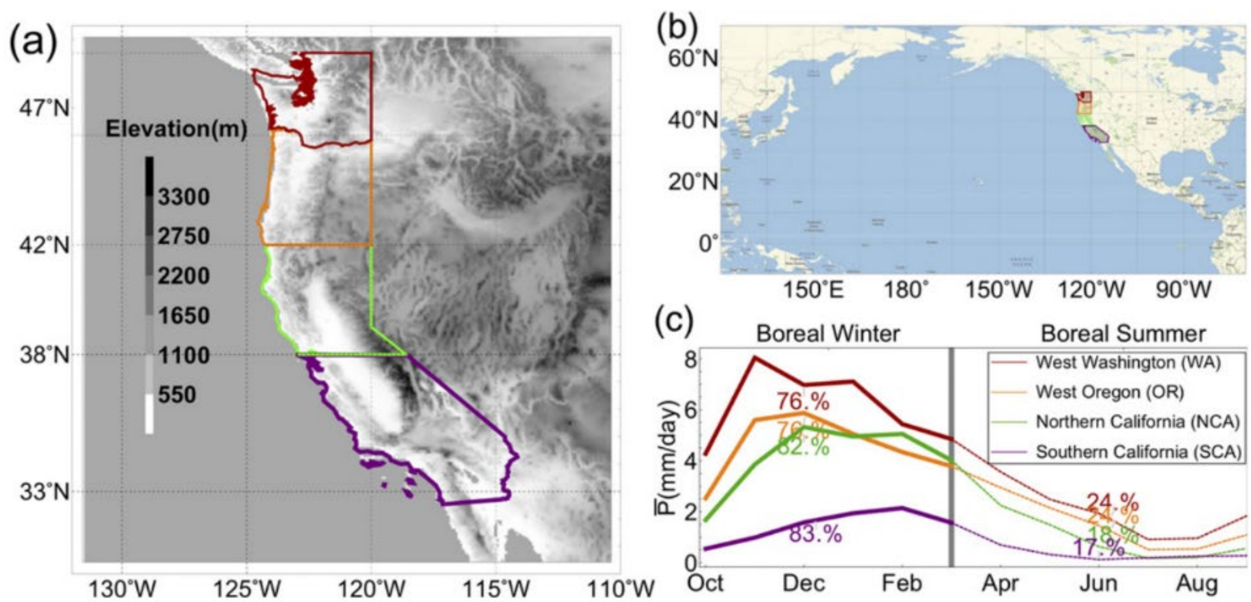

(a) The geographic map of the West Coast. (b) Geo-position of the study area in a global scale. (c) Monthly mean precipitation rates for the four subdivisions

Source: Pan et al., 2019a

In this study, the impact of the leading modes of intra-seasonal-to-seasonal variability on the distribution and prediction skill for precipitation forecasting was explored. The intention was to use the results as a baseline for follow-up investigations of seamless weather and climate predictions, ranging from one day to two months. The evaluation was based on extended-range retrospective forecast (hindcast) experiments developed by 11 operational centers (the 11 experiments are color coded in Figure 6) and hosted by the World Weather Research Programme and the World Climate Research Programme S2S Prediction Project Science Plan (Vitart, 2017).

The abundance of hindcast cases and model diversity offer an unprecedented opportunity for investigation of the potential predictability and prediction skill of precipitation. The specific experiments were to:

1. Evaluate the prediction skill for West Coast precipitation during the cold season in each general circulation model, on time scales from short to extended ranges.
2. Investigate the influence of intra-seasonal and seasonal variability on precipitation prediction skill in the general circulation models at the extended range, with emphasis on El Niño–Southern Oscillation (ENSO) and the Madden–Julian oscillation (MJO).

Using different spatial and temporal scales, four experiments were carried out based on:

1. **Daily Grid-Point-Scale Evaluation:** Evaluate the nth day prediction skill at each grid point (0.20° × 0.25°), n ranges for the entire period of forecast. The overall skill for each climate division is calculated by averaging skill scores for all the grid points within this division.
2. **Daily Regional-Scale Evaluation:** Evaluate daily regional average forecasts for each geographical division.
3. **Variable Temporal Windows, Grid-Point-Scale Evaluation:** Evaluation is carried out, following the strategy of Zhu (2014), at each grid point for various windows of lead time.
4. **Variable Temporal Windows, Regional-Scale Evaluation:** For each geographical division, the regional average precipitation forecasts are evaluated for variable windows of lead time.

Figure 6 shows the Pearson correlation coefficient between the ensemble mean of precipitation predictions and the observations for the four experiments. The evaluation results for Southern California and Northern California are shown in rows 1 and 2, respectively. The columns represent different experiments. The first column shows daily grid-point-scale evaluation results, the second column shows daily regional-scale evaluation results, the third column shows the variable temporal windows and grid-point-scale evaluation results, and the fourth column shows the variable temporal windows and regional-scale evaluation results.

For day-to-day evaluations (first two columns), as expected, each model showed a rapid decrease of r skill (r is the Pearson correlation coefficient that quantifies the linear correlation) with forecast lead times. Generally, because of the model performance differences, r fell below 0.2 within 8 to 15 days for Experiment 1 and 10 to 16 days for Experiment 2. A comparison between columns 1 and 2 showed that with a lead time of as much as two weeks, regional average predictions generally had higher r skill compared with grid-scale predictions. The skill improvements through spatial averaging were most obvious for Southern California, which is attributable to the uneven precipitation distribution for this region.

Figure 6: Estimated Pearson Correlation Coefficient

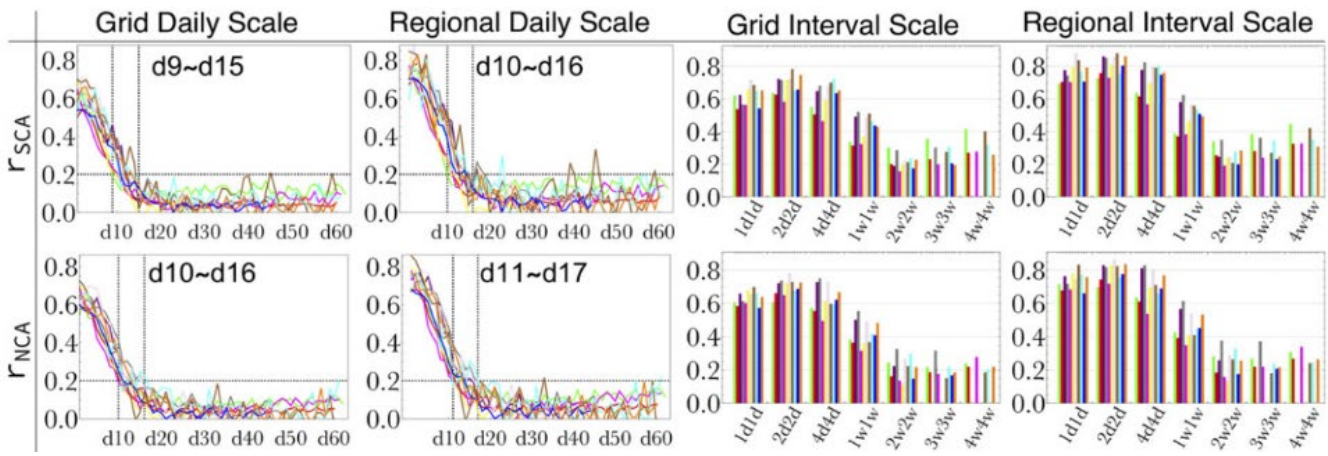

The estimated Pearson correlation coefficient r between ensemble mean predictions, and observations for the four experiments

Source: Pan et al., 2019a

For the temporal interval evaluation (last two columns), the statistics of best and mean performances at different windows of lead time are shown in Table 2 in APPENDIX A. Within the synoptic range, Day 2 (1d1d), days 3 to 4 (2d2d), and days 5 to 8 (4d4d) r skills are generally of the same order of magnitude (above 0.6 at grid scale and 0.7 at regional scale). This indicates that the decrease of prediction skill as lead time increases is compensated by the expanding of evaluation windows following the (*ndnd*) temporal averaging strategy. The Japan Meteorological Agency (JMA), Korean Meteorological Agency, Environment and Climate Change Canada (ECCC), and European Centre for Medium-Range Weather Forecast (ECMWF) models have the best performances at this temporal range. It is important to note that these models are of higher resolution when compared with the others. For Week 2 (1w1w), there is large variability in the models' r skills. The best-performing model (ECMWF) achieved an r skill of approximately 0.5 at grid scale, and 0.6 at regional scale. The average performance for all models was on the order of 0.4 for both grid and regional scales. Beyond two weeks, the models generally showed little usable skill. However, it is noteworthy that some models showed unexpectedly good performance at this time range, such as the Australian Bureau of Meteorology model for Southern California and the Hydrometeorological Centre of Russia model for Western Washington.

For Week 1, the S2S models showed advantageous precipitation prediction skills: the Pearson correlation coefficient (r), the Nash–Sutcliffe model efficiency coefficient (NSE), and the relative operating characteristics (ROC) score. The ROC score provides a summary of the hit ratio and false alarm ratio for different observation intervals. ROC scores were approximately on the order of 0.8, 0.7, and 0.8, respectively, for this period. By spatial averaging, the skill score can be further improved. For Week 2, models showed large variations regarding their performances. The Week-2 mean precipitation forecast from the best-performing model (ECMWF) was of considerable value, with r > 0.6, NSE > 0.35, and ROC score > 0.7. Beyond Week 2, predictions generally provided little deterministic skill. For this range period, the probabilistic evaluation of ensemble forecasts, using the continuous-ranked probability score, showed the significant advantage of ensemble forecasts over deterministic forecasts.

Considering the performance difference of the S2S models, the informative predictable range may differ by up to six or seven days between different models. In the short range, models with higher resolutions tended to have better performances. For the medium to extended ranges, ensemble mean predictions showed significantly better performance when compared with deterministic predictions. The best-performing models for this range period were the ECCC, ECMWF, and JMA models. For the Week 3 and Week 4 forecasts, although there was essentially no useful deterministic forecast skill, the ECMWF model still showed an advantage over the other models. These results can benefit model selections for both practical forecasts and multi-model ensemble predictions.

In conclusion, it was found that periods of heavy precipitation associated with the ENSO were more predictable at extended range periods. During El Niño years, Southern California tends to receive more precipitation in late winter, and most models show better extended-range prediction skill. On the contrary, during La Niña years Oregon tends to receive more precipitation in winter, with most models showing better extended-range skill. The team believes that the excessive precipitation and improved extended-range prediction skill are caused by the meridional shift of baroclinic systems, as modulated by ENSO. Through examining precipitation anomalies conditioned on the Madden–Julian oscillation, it was verified that active Madden–Julian oscillation events systematically modulate the area's precipitation distribution.

Enhancing Short-Term Precipitation Forecast Based on Long Short-Term Memory (LSTM) Recurrent Neural Networks
(Akbari Asanjan, 2018)

This study introduced a precipitation-forecasting algorithm with the potential to become an accurate short-term precipitation forecasting product, in quasi-global coverage. The CTBT data set from Geostationary Operational Environmental Satellite (GOES) is a homogenous and continuous data set used instead of directly using precipitation data. When compared with the rainfall data, the CTBT data obtained from the GOES satellites provided continuous values for each pixel and less randomness in each pixel's time dependencies as temperature changes followed the continuity governing law of heat transfer. The proposed approach was an advanced deep learning algorithm, termed Long Short-Term Memory (LSTM), to forecast the next time step of CTBT images from IR channel of GOES satellites. The algorithm then iteratively fed the forecasted CTBT image as input to obtain precipitation forecasts up to six hours ahead of time. Figure 7 depicts the LSTM algorithm concept. LSTM is a complex recurrent model developed by Hochreiter and Schmidhuber (1997) to address the deficiencies of recurrent neural network (RNN). LSTMs consist of one or more memory blocks as their fundamental units; the memory blocks contain memory cell(s) and gates that control the system's information flow. As shown in Figure 7, an LSTM block consists of an input gate, a forget gate, a memory cell, and an output gate.

Figure 7: Long Short-Term Memory

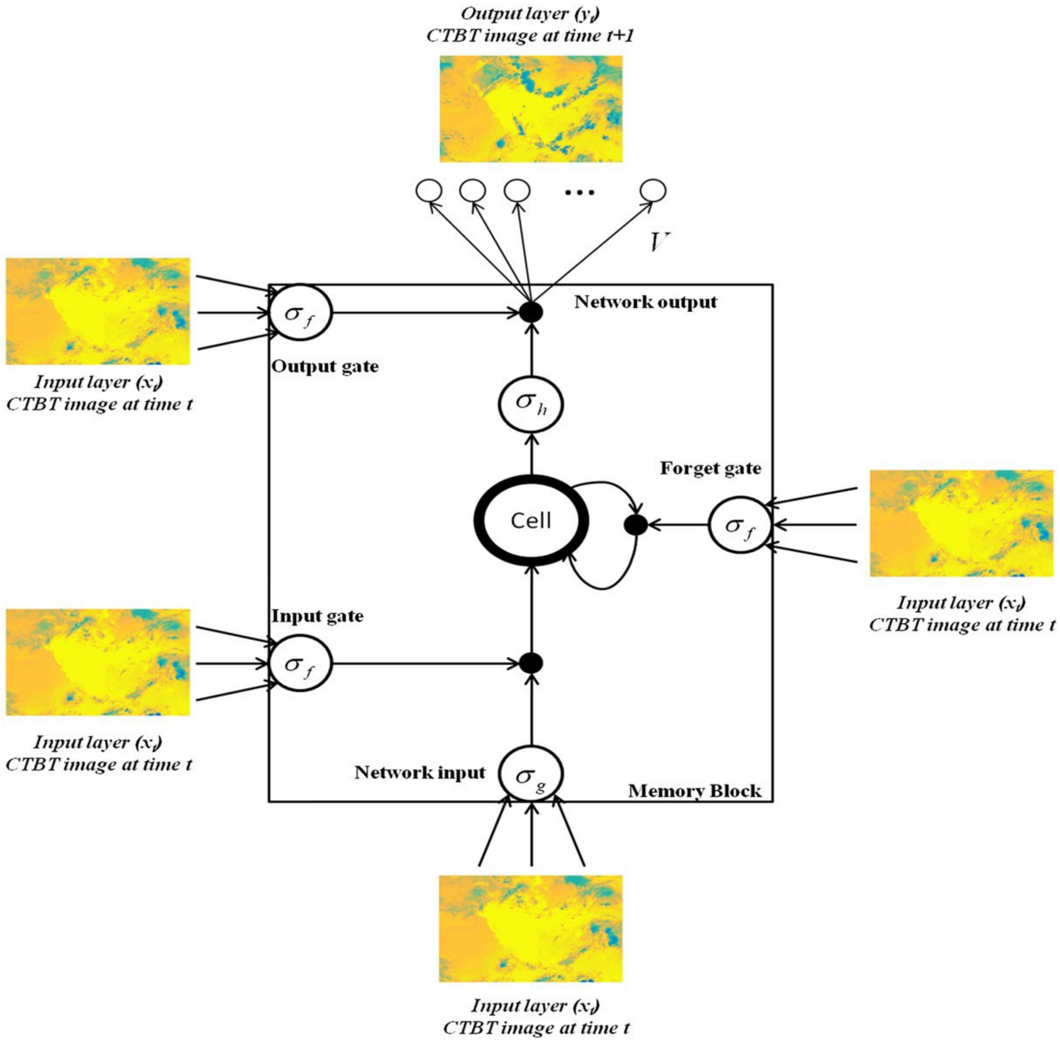

Source: Akbari Asanjan, 2018

The results from the proposed LSTM method are compared with a number of classical extrapolation-based methods including the RNNs, the Farneback Optical Flow method, and the Persistency method. These experiments indicate better statistics, such as correlation coefficient and root-mean-square error, for the CTBT forecasts from the proposed LSTM compared with the RNN, Persistency, and Farneback methods. The precipitation forecasts from the proposed LSTM and PERSIANN framework have demonstrated better statistics compared to the Rapid Refresh (RAPv.1), numerical forecasts and PERSIANN estimations from RNN, Persistency, and Farneback projections in terms of probability of detection, false alarm ratio, critical success index, correlation coefficient, and root-mean-square error, especially in predicting convective rainfalls. The proposed method shows superior capabilities in short-term forecasting over compared methods and has the potential to be implemented globally as an alternative short-term forecast product. Different precipitation patterns over the United States were identified using the model. The states of Oregon, Oklahoma, and Florida were chosen for case studies because of their different rainfall patterns. (Oregon: frontal, Oklahoma, and Florida: convective). It is also important to note that Oregon had dominant orthographic precipitation (like California); the new extension covers all of CONUS, which will deliver credible precipitation information for California as well. Figure 8 shows statistical results, the first row shows the RMSE and correlations for IR forecasts where LSTM (red line) is doing better than other models. The rest are statistics regarding corresponding precipitation in which LSTM is showing higher performances for the state of Oregon.

Figure 8: Mean CTBT and Precipitation Forecast Statistics Event-Based Performances for Oregon, for Six Hours

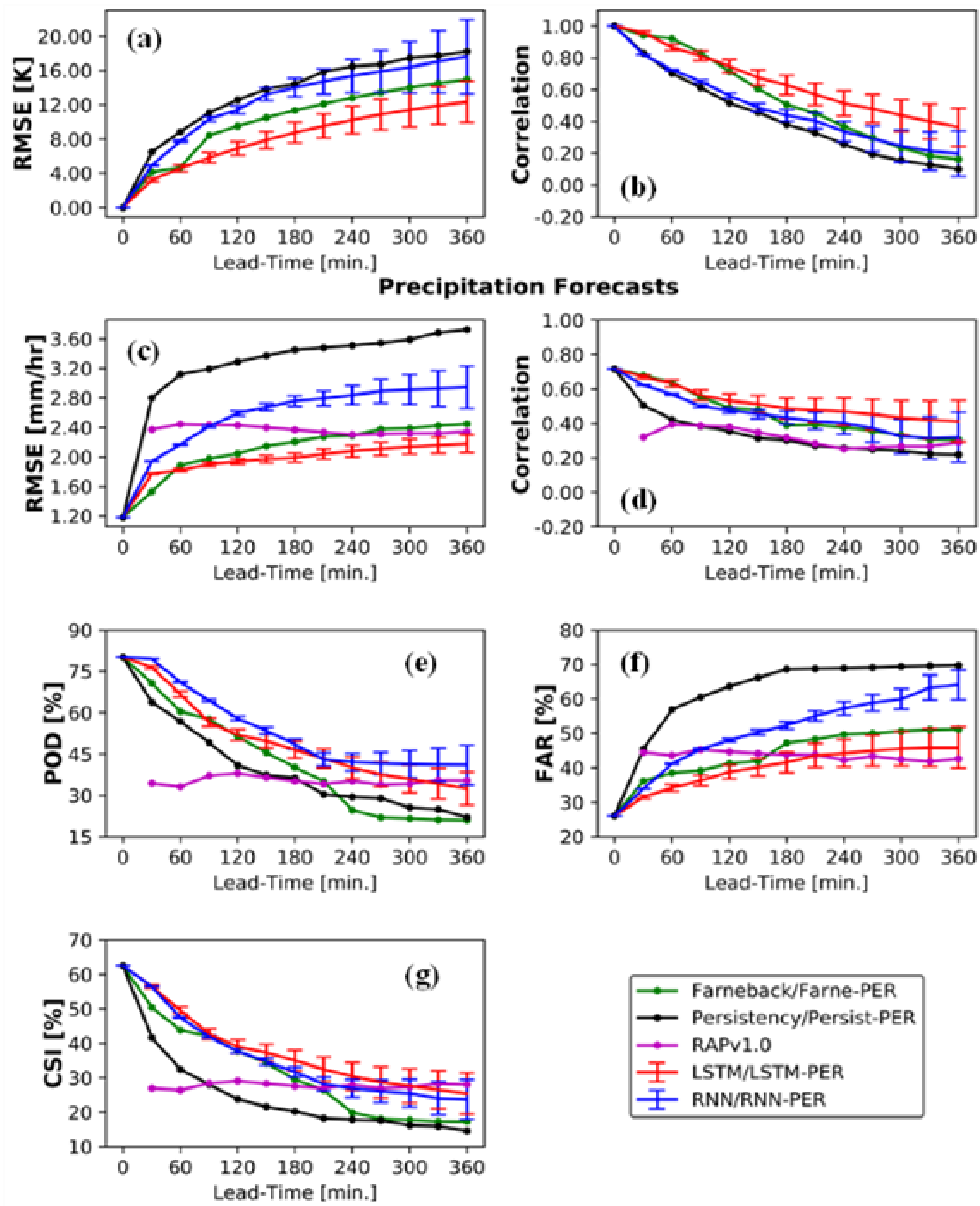

Source: Akbari Asanjan, 2018

Precipitation Estimation

Improving Precipitation Estimation Using Convolutional Neural Network
(Pan et al., 2019b)

To represent the precipitation process more accurately in comparison with numerical weather/ climate models and statistical downscaling methods, a convolutional neural networks (CNN) model was introduced. Specifically, the predictors were restricted to the variables that were directly derived from atmospheric dynamic equations. The model was directed to learn precipitation-related dynamical features from the surrounding dynamical fields by optimizing a hierarchical set of spatial convolution kernels. The model was tested at 14 geogrid points across the contiguous United States. The architecture of the proposed model and the map of studied climate zones are shown in Figure 9 and Figure 10.

Figure 9: The Proposed CNN Architecture

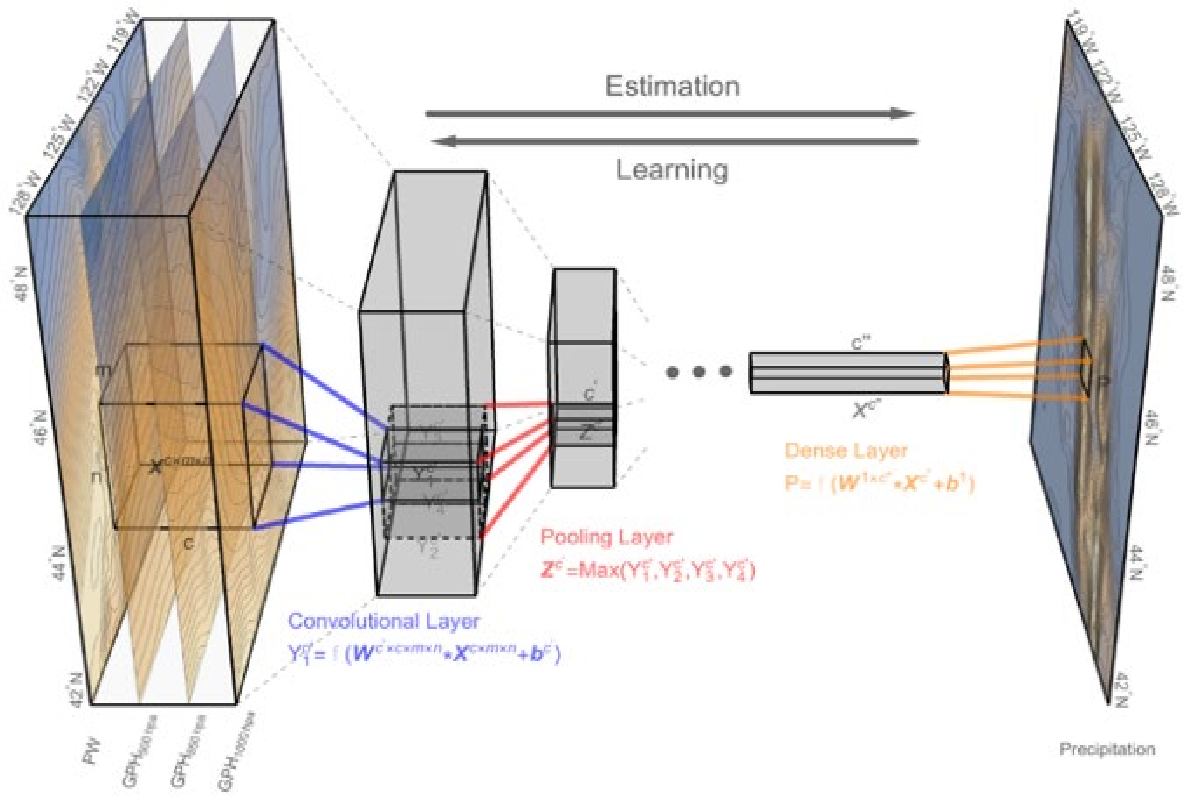

The CNN architecture for estimating precipitation using the numerical model resolved geopotential height and moisture field.

Source: Pan et al., 2019b

Figure 10: The Sample Grids Used in the Experiment

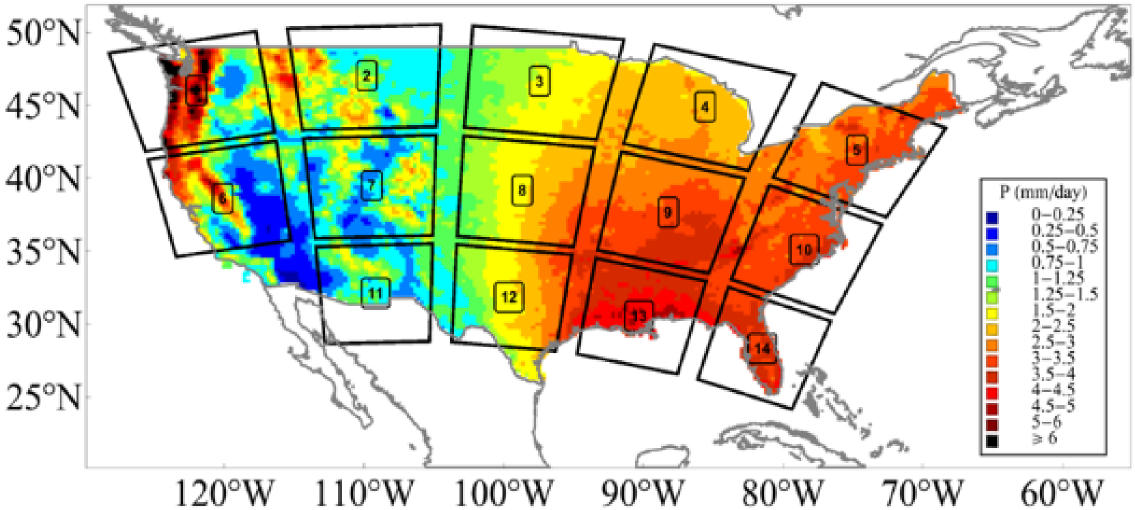

For each grid, the surrounding 800km x 800km dynamical field is delineated. The color indicates the mean daily precipitation rate averaging NOAA CPC daily precipitation. Records 1979-2017.

Source: Pan et al., 2019b

Results show that the CNN model outperforms the original North American Regional Reanalysis (NARR) precipitation estimates for the west and east coasts, where precipitation is more copious compared to other areas. For the middle part of the continent, the CNN model shows slightly worse performance, which can be attributed to model overfitting when there are limited precipitation samples for training the model.

In Figure 11, the scatter plots compare the precipitation estimation from CNN divided by precipitation estimation from NARR (P_{CNN} /P_{NARR}) against the CPC precipitation records (P_{obser}) for 6 of the 14 sample points regions.

The skill scores of r and RMSE for each point are given in corresponding sub-figures. The bold and underlined value indicates the better statistics of the two estimates. The bottom right geographic map shows the geoposition of the 14 points. The point is labeled red/blue if both skill scores indicate that P_{CNN}/ P_{NARR} perform better. It is labeled gray if the two skill scores show disagreement. For Region 6, including California, improvement in the PCNN estimates was observed.

Figure 11: Comparing PCNN(red)/PNARR(blue) Against CPC Precipitation Recodes (Pobser)

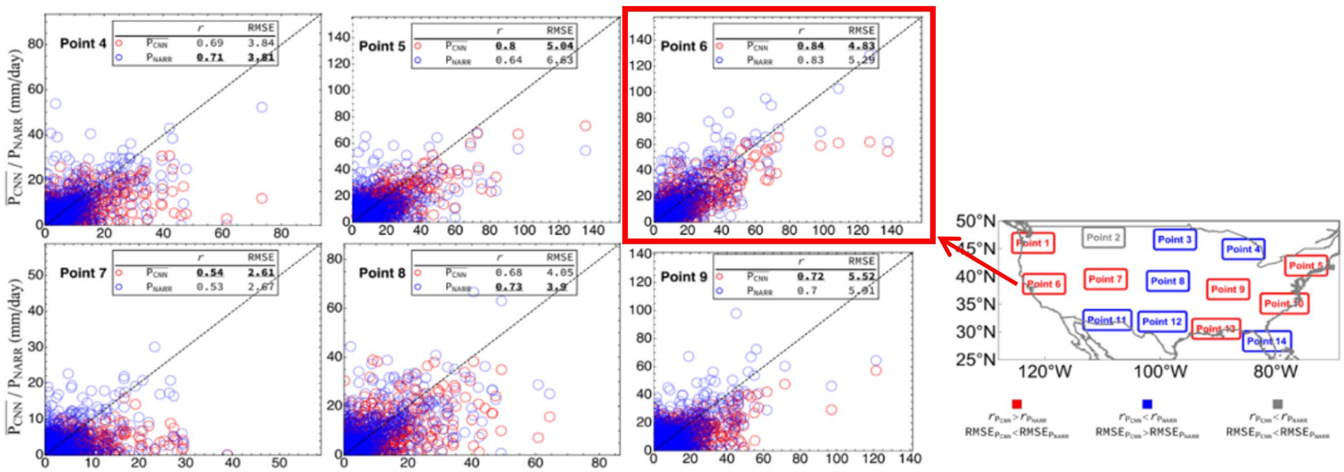

Source: Pan et al., 2019b

Through the case study of precipitation estimation, it was demonstrated that the CNN is a promising approach for climate downscaling. This model can seamlessly be incorporated in numerical precipitation predictions. Compared to the raw precipitation product from numerical models, the CNN model showed enhanced precipitation estimation when trained with abundant data. The performance improvement provided important implications for improving precipitation-related parameterization schemes using a data-driven approach. Through comparing the performance between CNN and fully connected neural network, linear regression, nearest neighbor, and random forest, the effectiveness of CNN for precipitation estimation was empirically verified.

Effective Cloud Detection and Segmentation Using a Gradient-Based Algorithm for Satellite Imagery: Application to Improve the PERSIANN-CCS
(Hayatbini et al., 2019a)

Effectively identifying clouds and monitoring their evolution are an important function for more accurate quantitative precipitation estimations and forecasts. In this part of the study, a new gradient-based cloud-image segmentation algorithm was developed using image processing techniques. This method integrated morphological image gradient magnitudes to separate cloud systems and patches boundaries. A varying scale kernel was implemented to reduce the sensitivity of image segmentation to noise and to capture objects with various fineness's of the edges in remote sensing images. The proposed method is flexible and extendable from single to multispectral imagery. In addition, case studies were carried out to validate the algorithm by applying the proposed segmentation algorithm to synthetic radiances for channels of the GOES-16 simulated by a high-resolution weather prediction model. Figure 12 shows the flow diagram for the proposed gradient-based segmentation algorithm.

Figure 12: Flow Diagram of Segmentation Algorithm

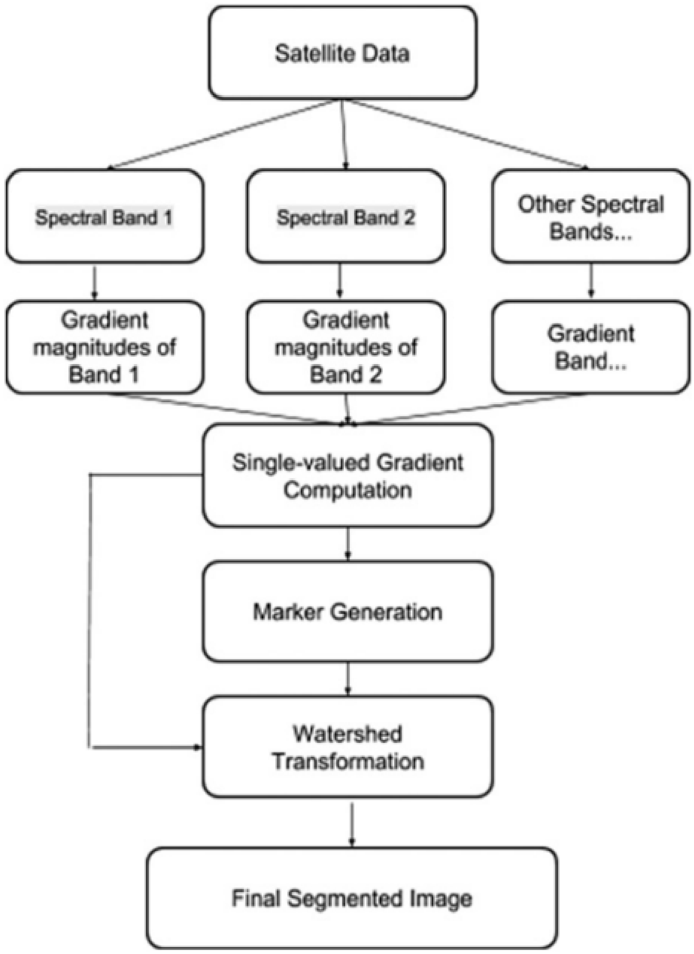

Source: Hayatbini et al., 2019a

The proposed method compared favorably with the existing cloud-patch-based segmentation technique implemented in the PERSIANN-CCS rainfall retrieval algorithm. The gradient-based segmentation result from simulated IR input along with gradient magnitude imageries of Hurricane Harvey event was studied. The gradient magnitudes were calculated from the IR images and the watershed segmentation was then applied to the gradient magnitude imageries based on the generated markers to achieve the final cloud patch segmentation. Figure 13 shows that the newly developed algorithm can capture more types of clouds, especially the warmer ones compared with the PERSIANN-CCS, in reference to the true cloud mask from the model simulations. This indicates that the gradient-based segmentation algorithm can overcome the drawback associated with threshold-based segmentation approaches implemented in patch-based precipitation retrieval algorithms.

Figure 13: Visual Comparison of Segmentation Algorithm

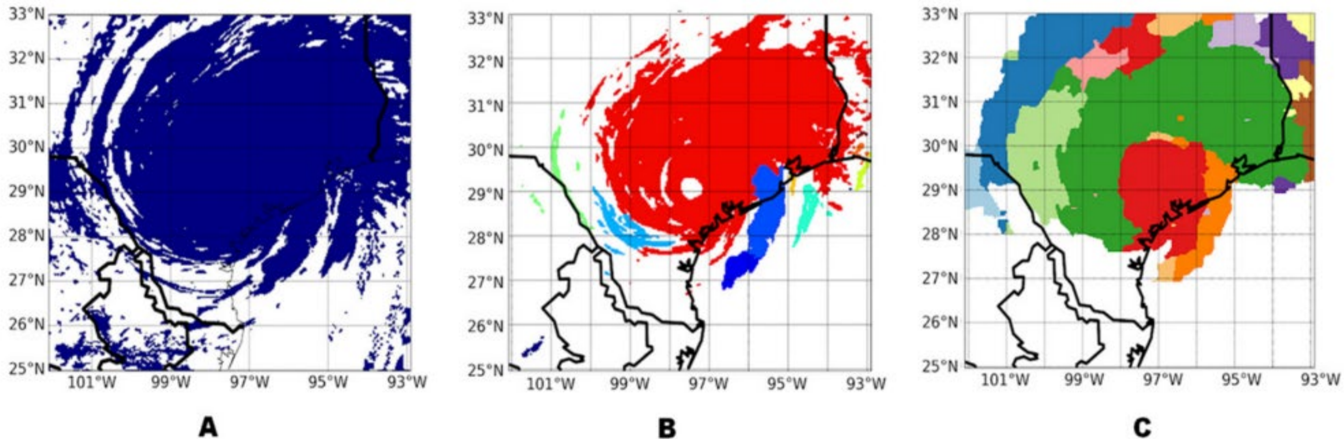

Visual comparison of the two segmentation outputs based on the truth mask as a reference for the simulated Hurricane Harvey event at 0300 UTC 26 Aug 2017. (A) Truth cloud mask used as a reference. The dark blue region implies the cloud existence. (B) PERSIANN-CCS segmentation result from single-IR channel. (C) Gradient-based segmentation algorithm output based on only the IR channel. In (B) and (C), each random color identifies a distinct cloud patch.

Source: Hayatbini et al., 2019a

In addition, Figure 14 compares the probability of detection (POD) and false alarm ratio (FAR) statistics of the proposed gradient based segmentation and PERSIANN-CCS algorithm. Constant improvements in segmentation skill using the gradient method algorithm are evident for Hurricane Harvey with its cloud systems evolving considerably in structure and morphology.

Evaluation of event-based images indicates that the proposed algorithm has superiorities when comparing to the conventional segmentation technique used in PERSIANN-CCS to improve rain detection and estimation skills with an accuracy rate of up to 98 percent in identifying cloud regions.

Figure 14: Statistical Comparison With PERSIANN-CCS

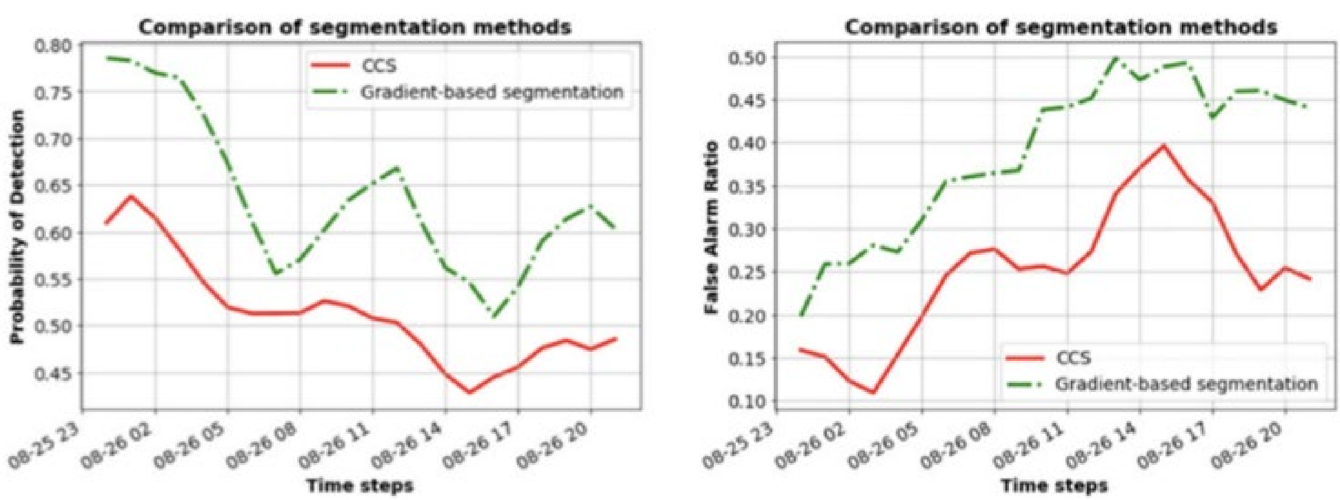

Statistical Comparison of Two Different Segmentation Algorithms for the Hurricane Harvey Case: (Left) POD, and (Right) FAR.

Source: Hayatbini et al., 2019a

Conditional Generative Adversarial Networks (cGANs) for Near Real-Time Precipitation Estimation From Multispectral GOES-16 Satellite Imageries—PERSIANN-cGAN

(Hayatbini et al., 2019b)

A state-of-the-art precipitation estimation framework which leverages advances in satellite remote sensing as well as Deep Learning is developed and verified. The framework takes advantage of the improvements in spatial, spectral, and temporal resolutions of the Advanced Baseline Imager onboard the GOES-16 platform along with elevation information to improve the precipitation estimates. This framework is proposed as an augmentation for PERSIANN-CCS algorithm for estimating global precipitation.

The procedure has two main steps. First, a rain/no rain (R/NR) binary mask through classification of the pixels is derived and a regression model to estimate the amount of rainfall for rainy pixels is applied. Secondly, a CNN is used as a regressor to predict precipitation estimates. The network is trained using the non-saturating conditional generative adversarial network (cGAN) and mean squared error (MSE) loss terms to generate results that better learn the complex distribution of precipitation in the observed data. The GAN concept is illustrated in Figure 15, where G is a generator network and D is a discriminator network.

Common verification metrics such as POD, FAR, Critical Success Index, rBIAS, Correlation and MSE were used to evaluate the accuracy of both R/NR classification and real-valued precipitation estimates. Statistics and visualizations of the evaluation measures show improvements in the precipitation retrieval accuracy in the proposed framework compared to the baseline models trained using only conventional MSE loss terms.

Figure 15: Schematic Conditional Generative Adversarial Network (cGAN) Structure

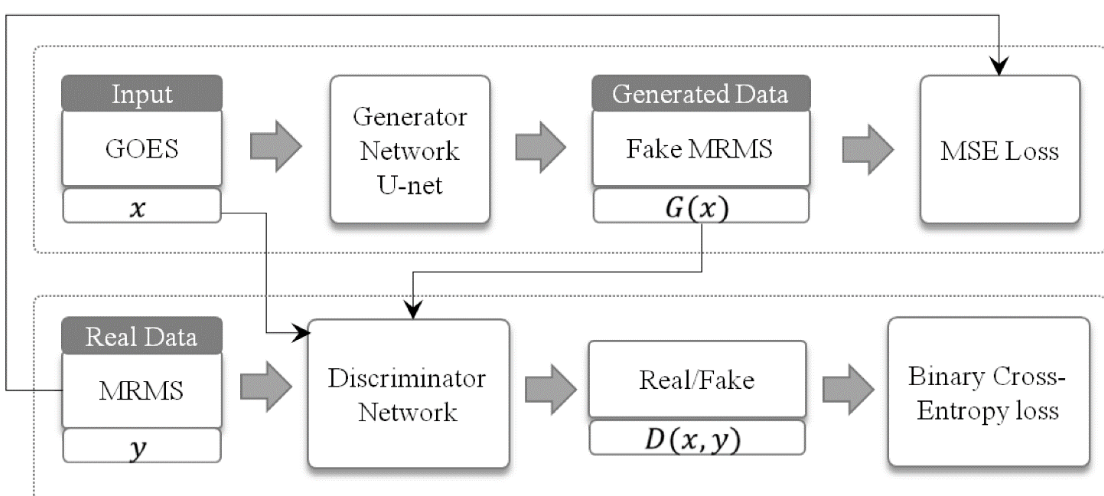

Source: Hayatbini et al., 2019b

The Multi-Radar/Multi-Sensor system (MRMS) data was used as the ground truth to investigate the performance improvement in both detecting the Rain/No Rain pixels and the rain estimates. Multiple channels were considered stand-alone and as the input to the proposed model including channel 13 with similar wavelength to PERSIANN-CCS to make the comparison fair. The elevation data was also considered as another input to the model, along with single bands of

Advanced Baseline Imager GOES-16 to investigate the effect of infusing elevation data as auxiliary information.

Figure 16 shows two sample IR band types and the half-hourly precipitation maps from the proposed cGAN model for July 31, 2018, at 22:00 — Coordinated Universal Time (UTC) along with the PERSIANN-CCS output and MRMS data for the same time step. Black circles on GOES-16 satellite imagery represent regions with warm clouds and the red circles are corresponding regions with rainfall associated with the warm clouds.

The visual comparison clearly demonstrates the superiority of PERSIANN-cGAN and improvement of precipitation estimates associated with warm clouds when compared to PERSIANN-CCS. The current investigation is a preliminary step as a proof of concept for global application and toward supporting the National Aeronautics and Space Administration's Global Precipitation Measurement Mission to develop effective multi-satellite precipitation retrieval algorithms for the fusion of precipitation information from multi-satellite platforms.

Figure 16: PERSIANN-cGAN Algorithm Results Visualization

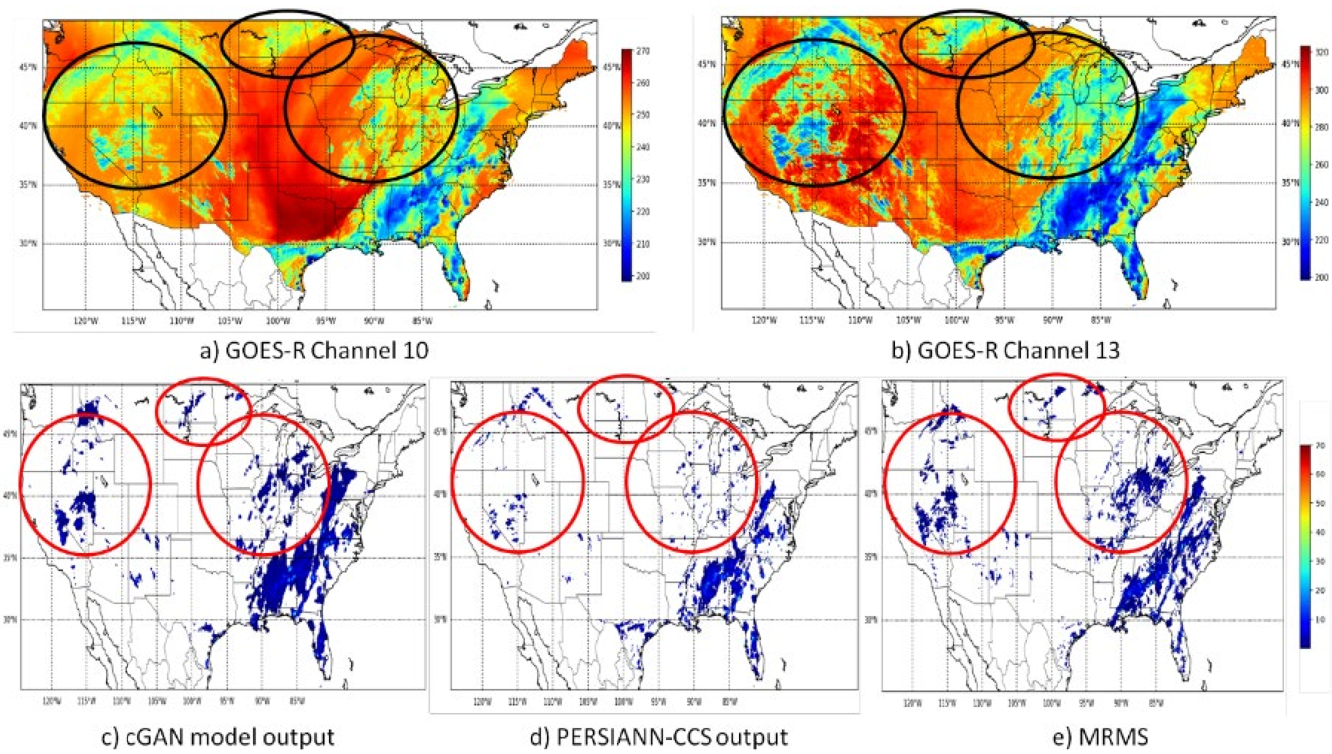

Source: Hayatbini et al., 2019

PERSIANN-CNN: Precipitation Estimation From Remotely Sensed Information Using Artificial Neural Networks–Convolutional Neural Networks
(Sadeghi et al., 2019a)

In this study the effectiveness of applying CNNs together with the IR and water vapor (WV) channels from geostationary satellites for estimating the precipitation rate were explored. The proposed model performances were evaluated over the central CONUS at the spatial resolution of 0.08-degree and at an hourly time scale. PERSIANN-CCS, which is an operational satellite-based product, and PERSIANN-stacked denoising autoencoder (PERSIANN-SDAE), were employed as baseline models. Results from the study demonstrated that the proposed CNN-based model (PERSIANN-CNN) can provide more accurate rainfall estimates compared to the baseline models at various temporal (hourly and daily) and spatial (0.08, 0.16, 0.25, and 0.5 degrees) scales.

Figure 17 shows an extreme storm that occurred on August 3, 2013, over the examined study area to compare the performance of PERSIANN-CNN against PERSIANN-CCS and PERSIANN-SDAE. On August 3, 2013, at 11:00 UTC, two separate cloud patches can be detected using the IR (a) and WV channels (b), which show intense rainfalls mostly near the central areas of the larger patch, as shown is sub-figure (c), which is the radar observation. As shown in Figure 17(e), PERSIANN-CNN provided a more realistic representation of the extent and the pattern of the rainfall patches when compared to PERSIANN-CCS (subfigure [f]) and PERSIANN-SDAE subfigure (d). Both programs falsely detected precipitation occurrence over the majority of the larger cloud patch where the cloud temperature was relatively lower.

Figure 17: Extreme Storm Event

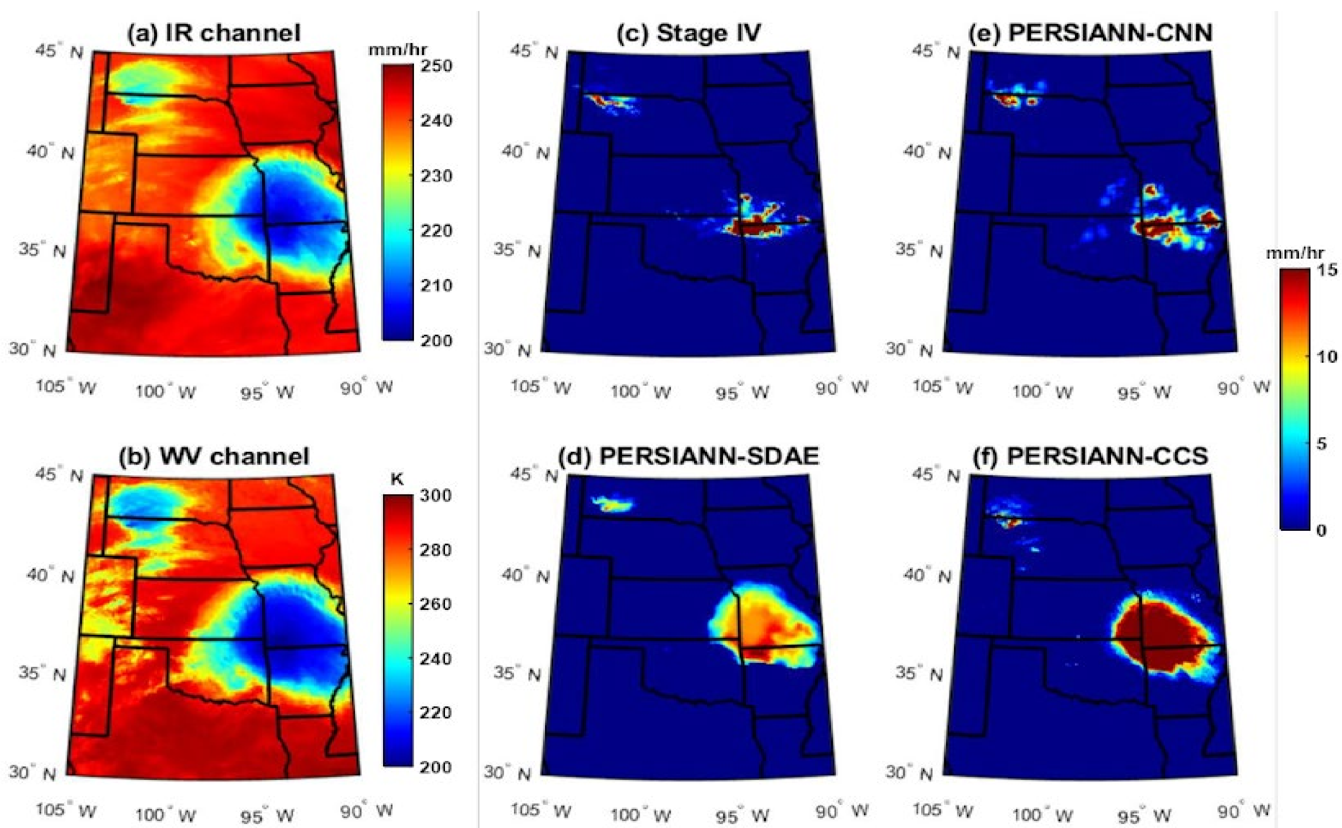

Source: Sadeghi et al., 2019a

Figure 18 additionally demonstrates how the proposed PERSIANN-CNN approach and baseline models performed in detecting and estimating the rainfall intensity throughout different evolution stages of the intense storm that occurred on August 3, 2013. Time series plots for the hourly rainfall estimates by the radar observations, PERSIANN-CNN, PERSIANN-CCS, and PERSIANN-SDAE, are shown. PERSIANN-CCS and PERSIANN-SDAE overestimated the rainfall for the entire event. However, PERSIANN-CNN's estimates corresponded well with the radar observations although there was a slight overestimation and underestimation before and after 11:00 UTC, respectively. The horizontal axis shows time steps (hr).

Figure 18: Rainfall Detection

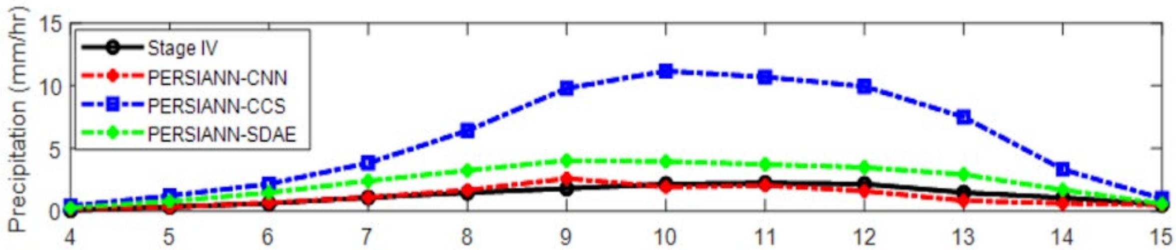

Source: Sadeghi et al., 2019a

Meta-Heuristic Optimization Applied to Reservoir Simulation Algorithms

Simplicity and flexibility of meta-heuristic optimization algorithms have attracted much attention in the field of optimization. Different optimization methods, however, hold algorithm-specific strengths and limitations, and selecting the best-performing algorithm for a specific problem is a tedious task. In this section, three optimization algorithms developed in response to the requirements of this project, with applications in reservoirs located in California are presented.

Shuffled Complex-Self Adaptive Hybrid EvoLution (SC-SAHEL) Optimization Framework

(Naeini et al., 2018)

The SC-SAHEL algorithm combines the strengths of different evolutionary algorithms (EAs) in a parallel computing scheme. The algorithm uses an "award and punishment" logic in junction with various types of EAs. SC-SAHEL explores performance of different EAs, such as the capability to escape local attractions, speed, or convergence, during population evolution as each individual EA suits differently to various response surfaces. The paper compares the performance of newly developed SC-SAHEL with a set of previously developed shuffled complex algorithms. The SC-SAHEL algorithm performance is evaluated on Folsom Reservoir, which is located on the American River, in Northern California. The main functions of the facility are flood control, water supply for irrigation, hydropower generation, maintaining environmental flow, water quality purposes, and providing recreational area. The reservoir has a capacity of 1,203,878,290 cubic meters and the power plant has a total capacity of 198.7MW. Three different periods are considered here. The first study period is April 1, 2010, to June 30, 2010. The year 2010 is categorized as below-normal period according to the California Department of Water Resources. The second and third study periods are over the April - June period selected in years 2011 and 2015, as the former is categorized by California Department of Water Resources as wet, and the latter is classified as *critical dry year*. The input and output from the reservoir are obtained from California Data Exchange Center.[2]

[2] http://cdec.water.ca.gov/

In Figure 19, the simulated storage for different study periods achieved by different EAs is presented. During the dry period (2015), not only the SC-SAHEL algorithm achieved the lowest objective function value, but also the storage level is higher than the observed storage level in most of the period. This is since power generation is a function of water height, as well as discharge rate.

Figure 19: Simulated Storage of Folsom Reservoir Simulated Storage for Dry (A), Below-Normal (B), and Wet (C) Periods

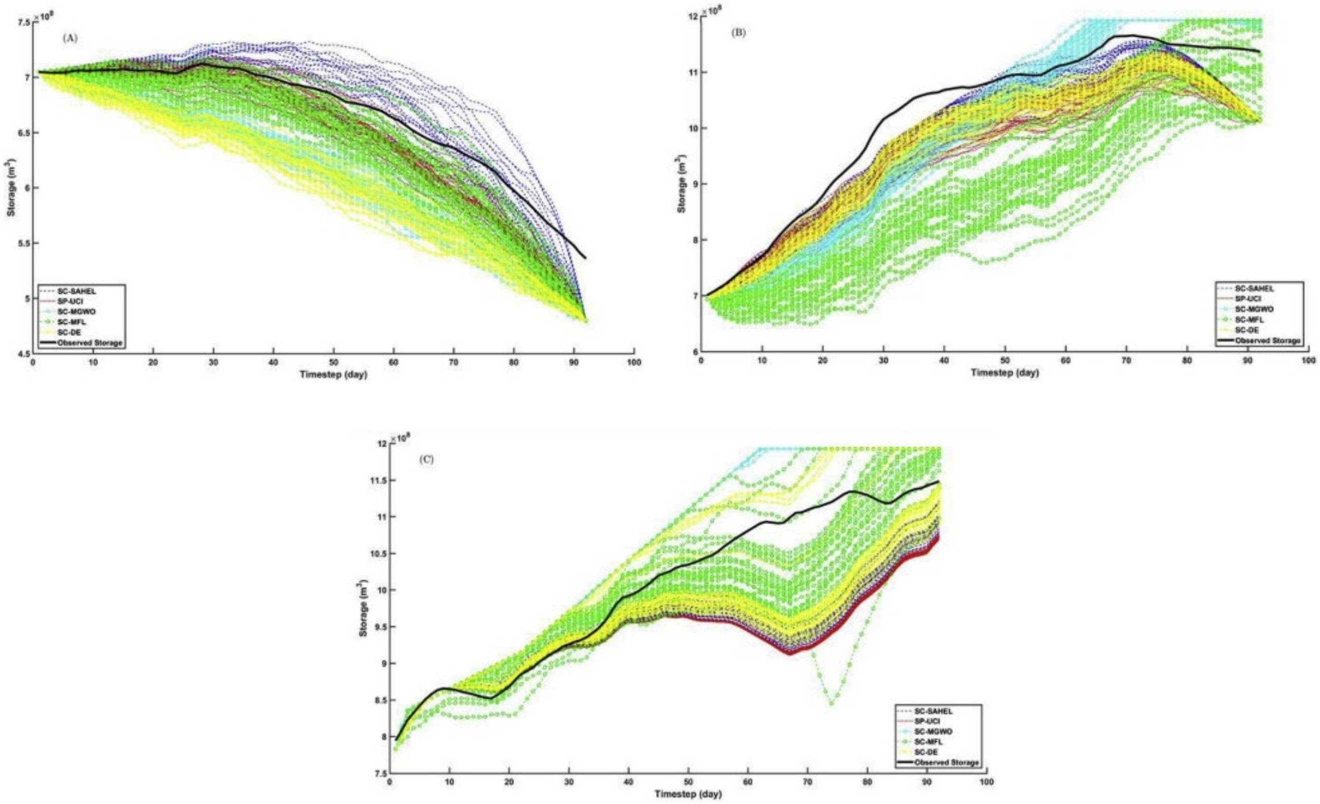

Source: Naeini et al., 2018

During the below-normal period, the algorithms SC-SAHEL, SP-UCI (shuffled complex strategy with principal component analysis developed at the University of California, Irvine), and shuffle complex-differential evolution (SC-DE) showed similar behaviors in terms of the storage level. During the wet period, the storage levels simulated by the SP-UCI and SC-SAHEL algorithms were lower than all other algorithms, however, in some of the runs they were able to find the optimum solution (objective function value is 0). However, the simulated storages by these algorithms showed some level of uncertainty, which showed equifinality in simulation, meaning that the same hydropower generation could be achieved by different sets of parameters.

The SP-UCI and SC-DE algorithms showed a similar behavior in terms of the storage level. During wet periods, storage levels simulated by the SP-UCI and SC-SAHEL algorithms were lower than all other algorithms. It is worth noting that, during the wet period, SC-SAHEL and SP-UCI algorithms were able to find optimum solutions (which objective function value is 0) in some of the runs. However, the simulated storages by these algorithms showed some level of uncertainty. This showed equifinality in simulation, meaning that same hydropower generation can be achieved by different sets of parameters.

The SC-SAHEL framework provided an arsenal of tools for testing, evaluating and developing optimization algorithms. The performance of the hybrid SC-SAHEL with single-method algorithms on 29 test functions was compared. The results showed that the SC-SAHEL algorithm is superior to most of single-method optimization algorithms and in general offers a more robust and efficient algorithm for optimizing various problems. Furthermore, the proposed algorithm can reveal the characteristics of different EAs during entire search periods. The algorithm is also designed to work in a parallel framework, which can take advantage of available computation resources.

A Model Tree Generator (MTG) Framework for Simulating Hydrologic Systems: Application to Reservoir Routing

(Naeini et. al, 2020)

Tree-based algorithms are transparent data-mining approaches that describe and present a response (dependent) variable by splitting the explanatory (independent) variables space into clusters of data. Simplicity and accuracy of tree-based algorithms make them attractive tools among practitioners in different fields of study including remote sensing, water resources management, and hydrology. Although classic tree-based algorithms were more concerned with classification and discrete spaces, application of tree induction methods have been extended to regression problems and continuous spaces. A wide range of algorithms have been proposed for regression tree induction, among which a classification and regression tree (CART), random forest (RF) and extremely randomized tree (Extra-Tree) found more applications in water resources management and reservoir studies. An extension to the regression tree algorithms is model trees (MTs), where the partitioning process is carried over according to a predefined measure of goodness for splitting candidates.

In addition, the exhaustive search mechanism embedded in MT algorithms can be biased in attribute selections where the number of possible split points is different for the attributes. Hence, the attributes with more split candidates have higher chances of being selected for partitioning. This search mechanism is also computationally inefficient for finding the combinatorial effect of variables. These shortcomings motivated the research agenda to develop a new generalized MTG framework for tree induction to reduce the selection bias and computation burden of MTs. They also enhanced the performance of these algorithms. Figure 20 shows a comparison between the sum squared residuals with respect to the mean setting, with single constant values in the terminal nodes (left plot) and the sum squared residuals using multiple linear regression setting with multiple linear regression in the terminal nodes (right plot) for generating models with the MTG framework. The figure also shows the superiority of linear regression to single constant values for representing subsets of data.

Figure 20: MTG Concept

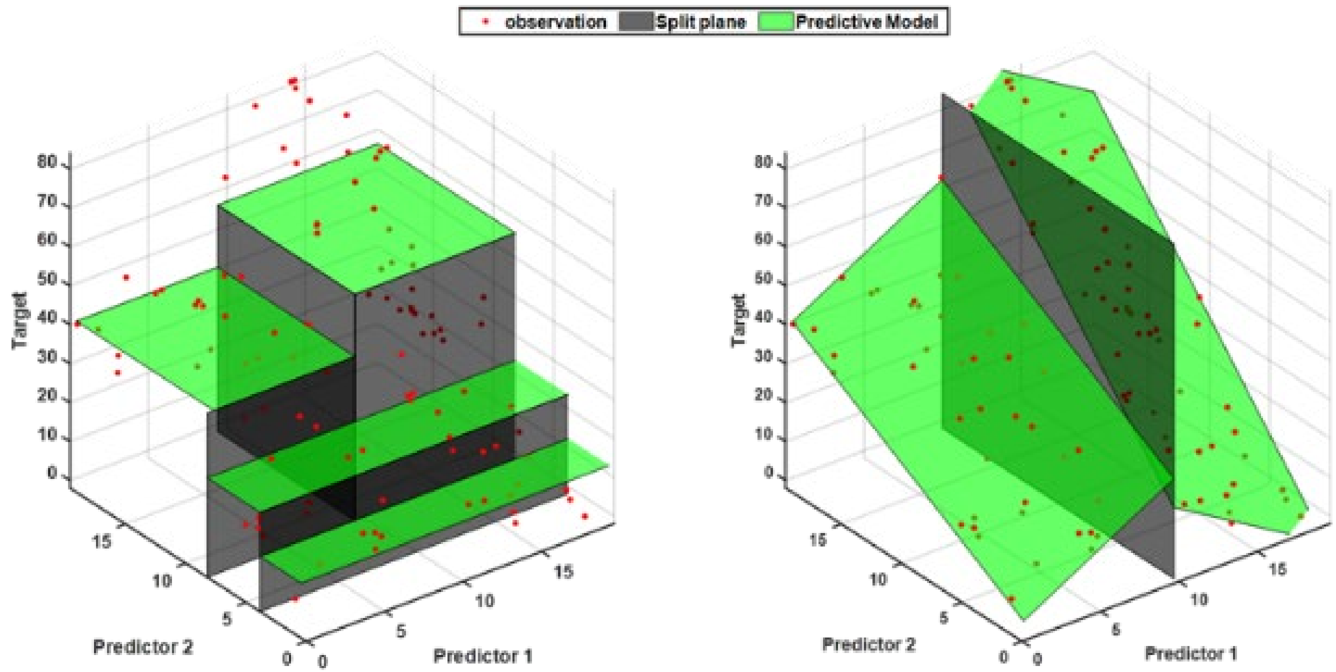

Source: Naeini et al., 2020

The MTG framework was employed to simulate daily discharge to evaluate the performance of the algorithms on rule-based hydrologic systems, as shown in Figure 21.

For this study, eight reservoirs with different ranges of services were selected. Figure 22 shows the location of these reservoirs across the CONUS. The selected reservoirs provide various services including flood control, water supply, recreation, and hydropower. Four of these reservoirs provide hydropower among which three of them are in California.

Figure 21: Reservoir Model Variables

Source: Naeini et al., 2020

Figure 22: Location of Case Study Reservoirs Over the Continental United States

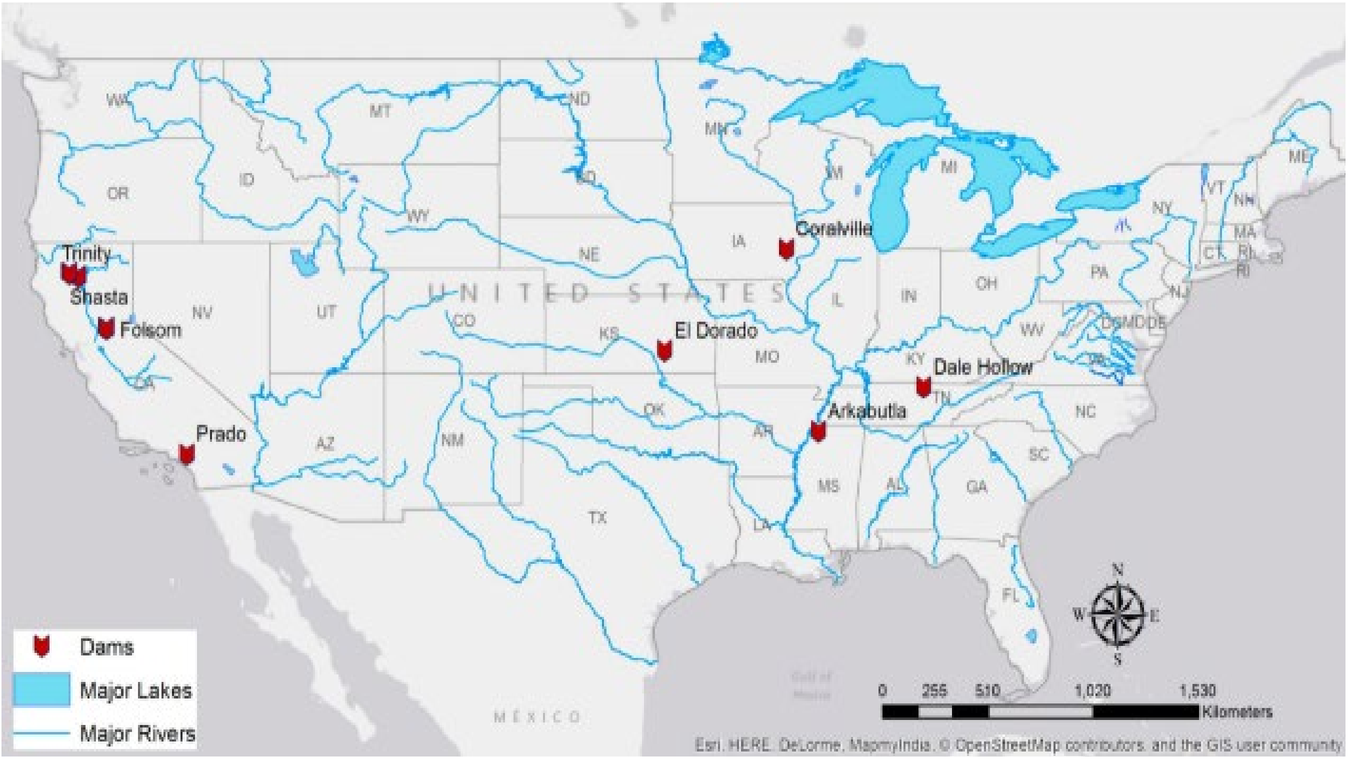

Source: Naeini et al., 2020

According to Figure 23, MTG(2) (which is MTG with sum squared residuals using multiple linear regression with quantile sampling) can better capture the peak flows and variability of data. Although the peaks are well simulated by MTG(2), the model overestimated low flows at the end of the period, due to the high inflow values. Similar behavior was observed for the M5 algorithm. The M5 algorithm maximized the expected error reduction and reduced the standard deviation. This can also be observed in the beginning of 2016 for all models. However, MTG(2) showed better performance for the whole period, specifically for the peak flows. The model generated by CART used constant values for flows and showed less variability for most flows. These results support the application of the MTs for reservoir routing and efficiency and effectiveness of the MTG framework for generating these types of models. Furthermore, the storage derived by the generated discharge with MTG model can better capture the variability of the storage for the whole period, in comparison to the CART and M5 algorithms. This is also evident from the correlation between the simulated and observed discharge and storage for the MTG(2) model.

Figure 23: Simulated Storage and Discharge for Shasta Dam

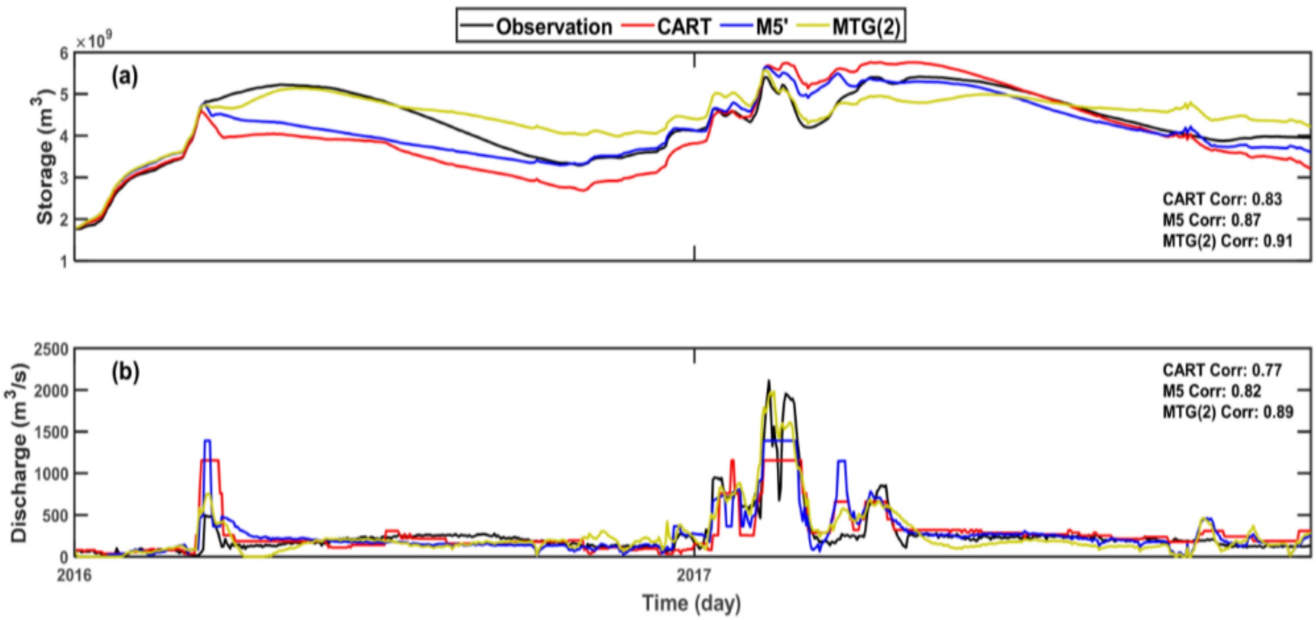

Simulated storage; (a) and discharge (b) for Shasta dam; years 2016 and 2017 using CART, M5′, and MTG(2) algorithms

Source: Naeini et al., 2020

Simulating Hydropower Discharge Using Multiple Decision Tree Methods and a Dynamical Model Merging Technique

(Yang et al., 2020)

Hydropower release decision-making relies on multisource information such as climate conditions, downstream water quality, inflow and storage, regulation and engineering constraints, and so on. The decision tree (DT) method is one of the commonly used techniques to simulate reservoir operation and release strategies because of its simplicity and effectiveness. However, the performances and simulation accuracy vary among different DT models due to many structures and splitting rules associated with each DT model.

In this study, a dynamic merge technique (DMerge), which adopts a concept from particle swarm optimization to postprocess outputs from different DT models, was proposed. The purpose of such approach was increasing the simulation accuracy and producing a model ensemble with dynamically changing weights throughout the validation phase. This new predictive approach, termed DMerge, is capable of using updated observation data to select the best ensemble members and is also capable of producing a more consistent and reliable prediction than any single DT model.

In addition, different DT methods in support of hydropower simulation using multiple information sources were compared and the importance of different model inputs, particularly water quality and climate information, with respect to the predictability of hydropower releases were evaluated. Figure 24 shows the concept of the DMerge technique. The core concept of this method is to use nonequal weights to dynamically create a single model averaging results with two specific models: the current best-performing model at Time Step t, and the historical best-performing model over the horizon from 0 to (t–1).

Figure 24: Dynamic Merge Technique

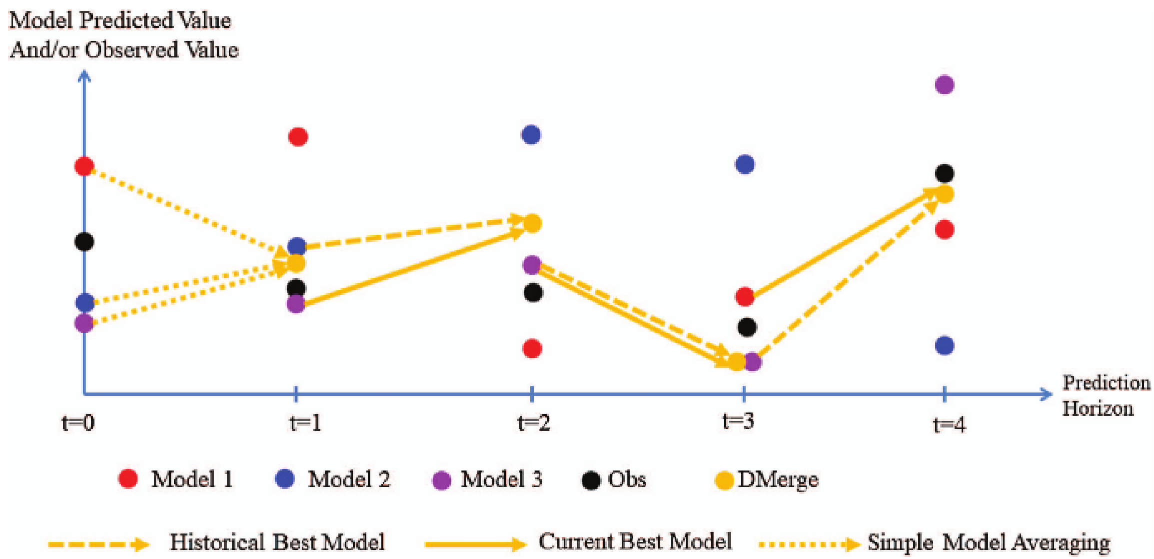

Source: Yang et al., 2020

The proposed technique is applied to Shasta Lake in northern California and the results are presented. The daily hydropower releases are predicted and compared using the DMerge, AdaBoost DT, random forest, and extremely randomized trees methods. These DT algorithms differ on how they handle splitting the data. According to Figure 25(a), all algorithms were able to produce reasonable simulations with a good match to observation. However, during February and March of 2015 in Figure 25(a), only the DMerge and AdaBoost algorithms were able to capture the sudden hydropower reduction, while other models overestimated the daily hydropower releases during this period. Another interesting phenomenon is shown during the period of June to October of 2015 in Figure 25(b), in which the AdaBoost tree algorithm significantly overestimated the hydropower releases. However, the DMerge method was able to capture the variation of hydropower releases and retains similar predictive performances to RF and the Extra-Trees algorithms, which are performing more satisfactorily than the AdaBoost tree algorithm during this particular prediction period.

Figure 25 shows the comparison between simulated and observed daily hydropower discharge under different scenarios during the validation period (January 1, 2014, to December 31, 2015). The observations are shown as black dots, and the red, blue, pink, yellow, and green lines represent the simulated discharges by AdaBoost, RF, Extra-Trees, simple model average (SMA), and the proposed DMerge method, respectively.

Figure 25: Comparing Simulated and Observed Daily Hydropower Discharges

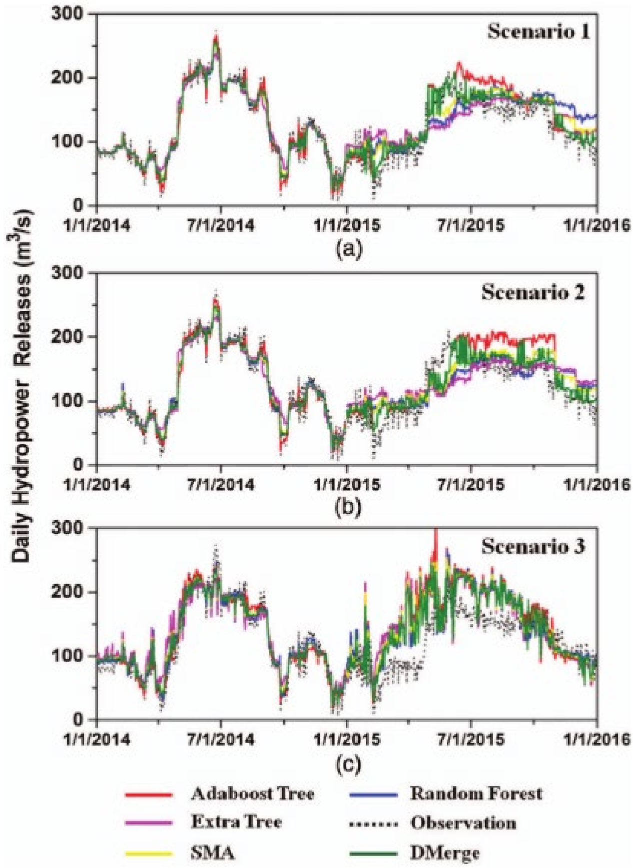

Comparison of observations (black dots) and predictions

Source: Analui and Sarooshian

As shown in Figure 26, 2010 to 2013 is used for calibration and 2014 to 2015 is used for validation period. Also, to compare the sensitivity of the model inputs, three different test scenarios were designed.

Figure 26: DMerge Model Setting, Designed Scenarios, and Modeling Structure

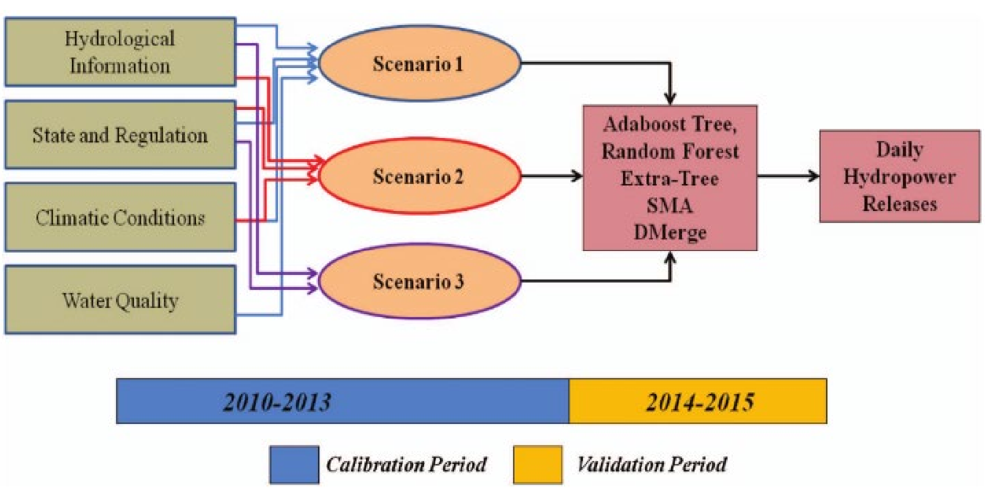

Source: Yang et al., 2020

Modeling Hydropower Scheduling Decisions

ARs usually result in massive rainfall along the coastline of California. While challenges remain over accurately estimating the associated rainfall, the wide coverage and high spatiotemporal resolution of the satellite precipitation products make them suitable for driving distributed hydrological models. In this section, the outputs delivered by PERSIANN family products were used as the main forcing input to a semi-distributed hydrological model to generate daily streamflow information. This information demonstrates the capability of improved PERSIANN products in more accurate streamflow modelling and simulation, which contributes to the increasing confidence and higher efficiency of hydropower scheduling decisions. With California the study region of this project, evaluation of PERSIANN precipitation products through streamflow simulation with a distributed hydrological model, the Weather Research and Forecasting Model Hydrological modelling system (WRF-Hydro), for a coastal watershed was studied.

Hydrologic Evaluation of PERSIANN Precipitation Products Through Streamflow Simulation Using WRF-Hydro

(Analui and Sarooshian)

The Russian River Basin is located within Sonoma and Mendocino counties in Northern California. The watershed has an area of 3,846 square kilometers and is surrounded by the Mayacamas Mountains to the east and the Coast Ranges to the west (Figure 27).

Figure 27: Russian River Watershed

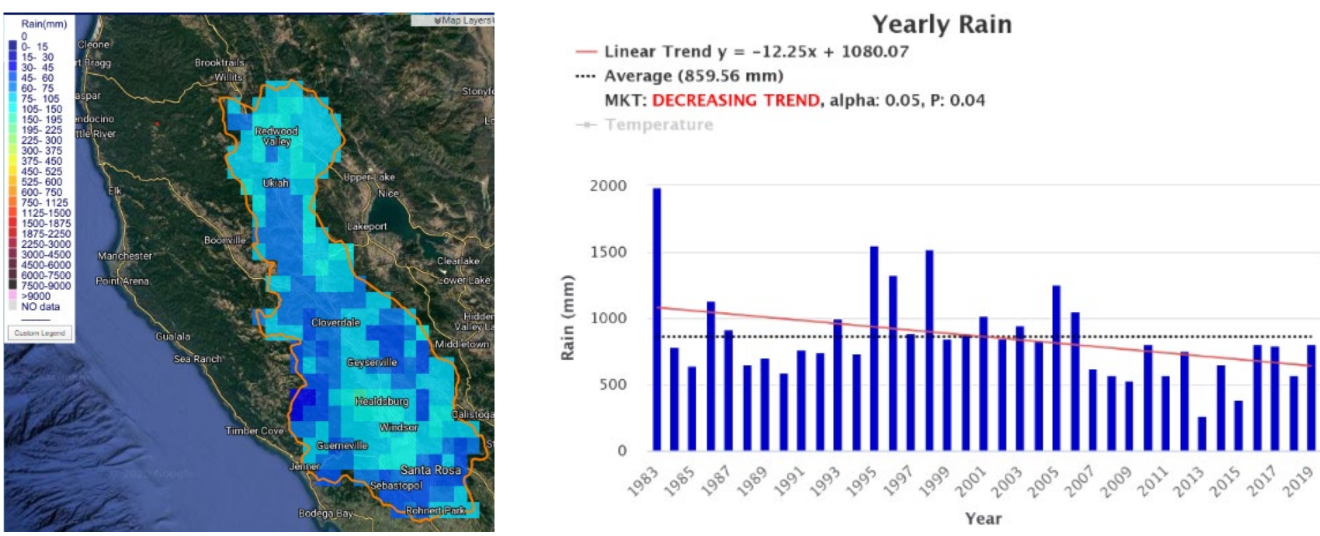

(Left) Monthly precipitation rate based on PERSIANN-CCS, January 2020. (Right) Annual precipitation rate obtained from RainSphere based on PERSIANN-CDR.

Source: Analui and Sarooshian

With a hot summer and wet winter, the annual mean precipitation rate from 1983 to 2019 is 859.56 mm, with 51 percent of the annual precipitation induced by atmospheric rivers (Ralph et al., 2013), which can cause flooding in extreme cases. There are two reservoirs within the basin for flood control: Lake Mendocino and Lake Sonoma. Figure 28 provides a visual depiction of the Russian River Watershed and the stream gauges, before and after both lakes, that gather important metrics such as flow rates and stream temperatures. The data collected from the gauges is used to allocate water during droughts, predict flooding events, ensure the protection of fish, and track illegal diversions.

Figure 28: Russian River Stream Gauges

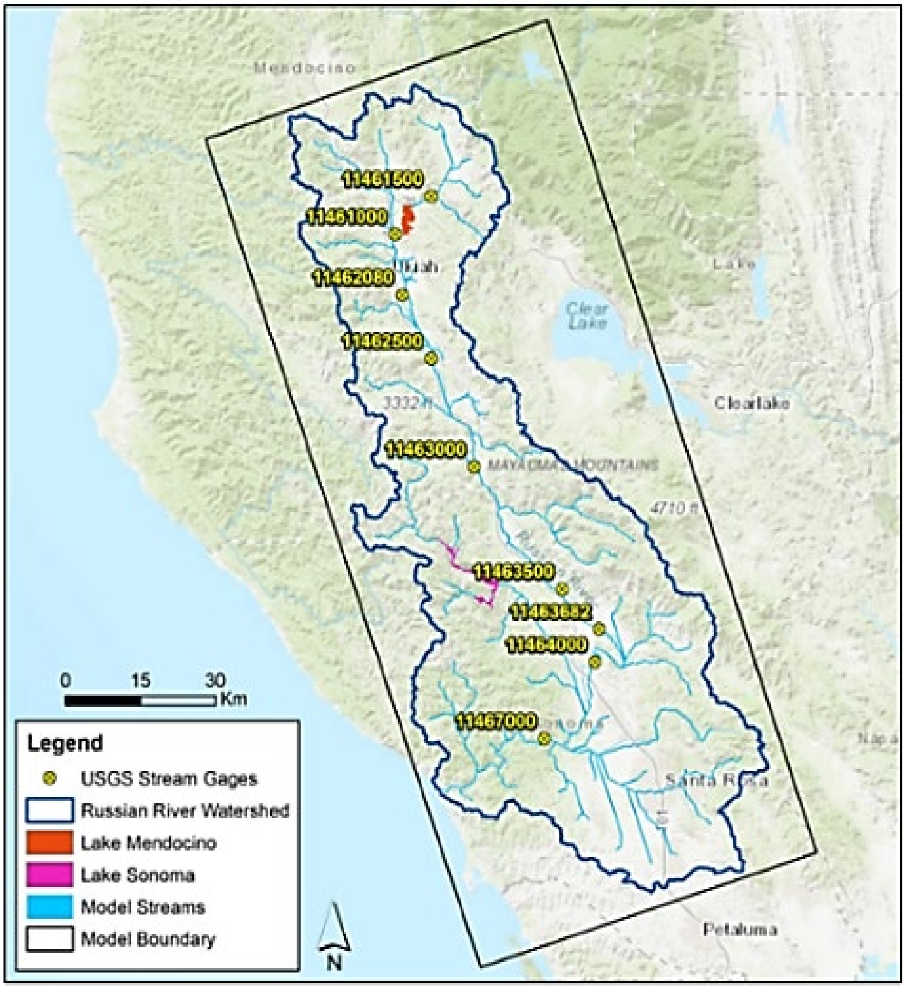

Source: Analui and Sarooshian

Precipitation Data

The evaluation is based on four satellite-based precipitation products from the PERSIANN family: the PERSIANN-CDR, PERSIANN-CCS, and the more recently developed PDIR-Now and the PERSIANN-Cloud Classification System-Climate Data Record (PCCSCDR) of hourly resolution. The benchmark used was a gage-corrected MRMS precipitation product. Table 1 summarizes the spatial and temporal resolutions, available periods, and coverage of the precipitation products. All precipitation products were re-gridded spatially to the 1000-meter resolution land surface model grid using bilinear interpolation and were resampled temporally to hourly resolution. For PERSIANN-CDR, the hourly precipitation was assumed to be the same within each three-hour interval. Figure 29 shows the hyetograph for MRMS and PERSIANN family precipitation products for water years (WYs) 2017 to 2019.

Table 1: Summary of the Precipitation Products Used in the Study

Dataset	Period	Spatial Resolution	Temporal Resolution	Coverage
MRMS (Gauge Corrected)	June 2006* - Present	0.01° x 0.01°	1-hourly	125°W to 25°E, 67°S to 53°N
PERSIANN-CDR	January 1983 - Present	0.25° x 0.25°	3-hourly	180°W to 180°E, 60°S to 60°N
PCCSCDR	January 1983 - Present	0.04° x 0.04°	3-hourly	180°W to 180°E, 60°S to 60°N
PERSIANN-CCS	January 2003 - Present	0.04° x 0.04°	1-hourly	180°W to 180°E, 60°S to 60°N
PDIR-Now	March 2000 - Present	0.04° x 0.04°	1-hourly	180°W to 180°E, 60°S to 60°N

***The MRMS only became operational in September 2014 but has been running in real time since June 2006. (Qi et al., 2016)**

Source: Analui and Sarooshian

Figure 29: Hyetograph for MRMS and PERSIANN Family Precipitation Product

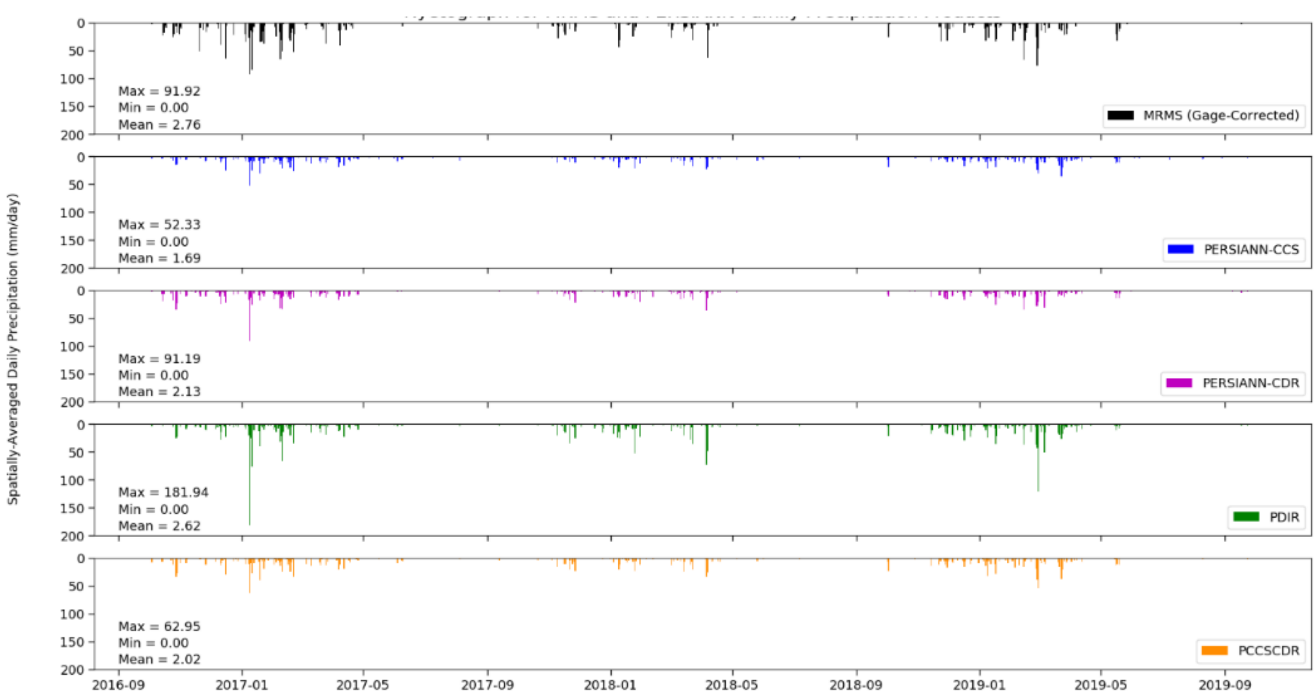

Calibration Period: 10/1/2016 to 9/30/2018 and validation period: 10/1/2018 to 9/30/2019

Source: Analui and Sarooshian

Method

The WRF-Hydro modelling system is a distributed modeling system that integrates multi-scale atmospheric and terrestrial hydrologic processes designed to be compatible with parallel computing applications (Gochis, 2020). Its architecture also allows for stand-alone hydrologic modeling without two-way coupling with the atmospheric component. WRF-Hydro has been successfully applied in various studies (Yucel, 2015), (Arnault, 2016) and (Verri, 2017). It constitutes the core of the United States National Water Model, which forecasts streamflows over the entire continental United States for nationwide decision support services.[3]

In this study, version 5.1 of WRF-Hydro was used and forced with prescribed atmospheric datasets (one-way coupling). The model comprises six modules: land surface model, subsurface flow routing, overland flow routing, baseflow model, channel routing, and reservoir routing. The evaluation was conducted after automatic model calibration for WY 2017 and WY 2018 in two different approaches, using either MRMS precipitation or each of the aforementioned PERSIANN products as inputs. The calibration was performed using a surrogate-based method and targeted 14 sensitive parameters. Further technical details on descriptions about WRF-Hydro modules and calibration process can be found in Appendix A.

Numerical Results and Analysis

These simulations assessed the effects of PERSIANN rainfall estimates on streamflow when WRF-Hydro was calibrated with the individual products. Figure 30 presents a time series comparison of the input specific-calibrated model simulations with observed daily streamflow. For the calibration period from WY 2017 to WY 2018, the PERSIANN family products were better able to reproduce the variability of the observed streamflow. Compared to the MRMS calibrated streamflow, there was a reduction in the overestimation by the PDIR-Now in February 2017. Notably, input-specific calibration allowed PERSIANN-CDR, PCCSCDR, and PERSIANN-CCS to approach the higher peak streamflows in January to May 2017, and May 2018, but also resulted in unintended spikes during other low streamflow periods, especially for PCSSCDR in November 2016. A similar performance was observed during the validation period in WY 2019.

Figure 30: Time Series Comparison of the Input Specific-Calibrated Model Simulations With Observed Daily Streamflow

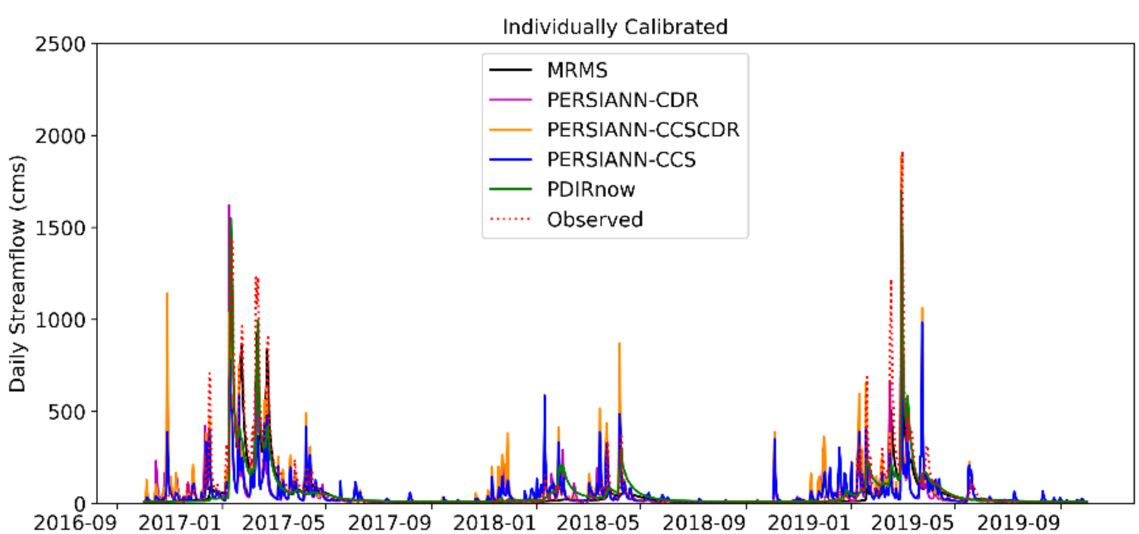

Source: Analui and Sarooshian

[3] https://water.noaa.gov/about/nwm, last access: 12 July 2020

The statistical comparisons for the validation period show that the performance generally improved for the PERSIANN family products, with PDIR-Now results being the closest to the observed streamflow. The bias remained negative but was substantially reduced for PERSIANN-CDR (-40 percent), PCCSCDR (-20 percent) and PERSIANN-CCS (-32 percent percent). The NSE for PERSIANN-CCS improved the most to a positive value of 0.31 but it was still lower than that of both PERSIANN-CDR (0.40) and PCCSCDR (0.36). The correlation coefficient for PERSIANN-CDR and PERSIANN-CCS improved to 0.69 and 0.58 respectively, but the correlation coefficient for PCCSCDR decreased from 0.71 to 0.61. The latter can be explained by the spikes induced after the calibration during the low streamflow periods. The outperformance of PDIR-Now over MRMS increased further in terms of NSE (0.71), RMSE (102.35), and rBIAS (-22 percent). While the correlation coefficient for PDIR-Now improved to 0.88 after input-specific calibration, it was slightly lower than that of MRMS (0.93).

CHAPTER 3: Conclusion

Precipitation measurements with high spatiotemporal resolution are a vital input for hydro-meteorological and water resources studies; decision-making in managing extreme weather events; and weather, climate, and hydrological forecasting. The focus of this research project was to develop advanced machine and deep learning mechanisms to improve the accuracy of an existing near real-time PERSIANN product. More specifically, this research developed a module that uses climatological data to construct a dynamic that:

- Has several notable advantages over other quantitative precipitation estimation algorithms.
- Has noteworthy skill over the CONUS (with specific improvement for challenging areas in western CONUS and California in particular).
- Employs machine learning algorithms to improve precipitation forecasts.

Previous research suggests that one of the main reasons for substantial errors in hydrologic forecasting is the lack of quality data on both temporal and spatial variations of historical precipitation. Therefore, this research, building upon the foundations of PERSIANN family, developed a new algorithm for estimation of precipitation rates from satellite IR radiation imagery, which offers notable advantages over current algorithms for rainfall estimation especially over the western Contiguous United States. The new algorithm PDIR-Now advances the framework of the existing PERSIANN-CCS system.

Moreover, since precipitation variability significantly influences the heavily populated West Coast of the United States, it raises the need for reliable predictions. Therefore, as part of this project, researchers investigated short-to-extended-range precipitation prediction skill in the West Coast of the United States. The study used the hindcast database of the S2S project. It was found that periods of heavy precipitation associated with the El Niño southern oscillation were more predictable in the extended range period than in the shorter time frame.

In addition, a range of advanced machine learning and neural network algorithms were developed to improve the PERSIANN family products and deliver precipitation estimation and short-term forecast more accurately by:

- Enhancing short-term precipitation forecasts based on LSTM recurrent neural networks. This study introduced a precipitation-forecasting algorithm that could potentially become an accurate short-term precipitation forecasting product in quasi-global coverage. The precipitation forecasts from the proposed LSTM and PERSIANN framework have demonstrated better statistics compared to the Rapid Refresh (RAPv.1), numerical forecasts and PERSIANN estimations from RNN, persistency, and Farneback projections in terms of probability of detection, false alarm ratio, critical success index, correlation coefficient, and root-mean-square error, especially in predicting convective rainfalls.

- Improving precipitation estimation using a CNN. In order to represent the precipitation process more accurately in comparison with numerical weather and climate models and statistical downscaling methods, a CNN model was introduced. Specifically, the predictors are restricted to the variables that are directly derived from atmospheric dynamic equations. It was found that the CNN model outperforms original NARR precipitation estimates for the west and east coasts, where precipitation is more abundant compared with other areas.
- PERSIANN-CNN: In this work the effectiveness of applying CNNs, together with the infrared and water vapor channels from geostationary satellites for estimating the precipitation rate, was explored. Results showed that PERSIANN-CNN's hourly rainfall estimates corresponded well with the radar observations, while other PERSIANN family models overestimated the rainfall for the tested rainfall intensity event.

Three generalized reservoir release and hydropower production models were also developed to leverage data-driven and meta-heuristic approaches. Finally, an analysis on streamflow simulation improvement and forecast accuracy was designed based on improved precipitation estimates, with application in California to assist hydropower management for a major operational facility serving in California.

The outcomes of this research provide decision makers with improved information regarding hydrologic modeling and short-term hydropower scheduling and will attempt to close the knowledge gap regarding the efficiency and reliability of forcing data in hydrological forecasts.

GLOSSARY AND LIST OF ACRONYMS

Term	Definition
AR	atmospheric river
ASMO-PODE	adaptive surrogate modeling-based optimization - parameter optimization and distribution estimation
CART	classification and regression tree
CCS	cloud classification system
CDR	climate data record
CEC	California Energy Commission
cGANs	Conditional Generative Adversarial Networks
CMORPH	Climate Prediction Center MORPHing technique
cms	cubic meters per second
CNN	convolutional neural networks
CONUS	contiguous United States
CORR	correlation coefficient
CPC	Climate Prediction Center
CTBT	cloud-top brightness temperature
DMerge	dynamic merge technique
DRAM	Delayed Rejection Adaptive Metropolis
DT	decision tree
EA	evolutionary algorithms
ECCC	Environment and Climate Change Canada
ECMWF	European Centre for Medium-Range Weather Forecast
ENSO	El-Niño-Southern Oscillation
EPIC	Electric Program Investment Charge
FAR	false alarm ratio
GCM	general circulation model
GOES	Geostationary Operational Environmental Satellite
hr	hour
JMA	Japan Meteorological Agency
IR	infrared
LSM	Land surface model
LSTM	long short-term memory

Term	Definition
M5	M5 is primarily used for supervised learning and produces either a decision tree or a tree of regression models in the form of simple linear functions.
MannN	Channel routing roughness coefficient
MJO	Madden-Julia oscillation
mm	millimeter
mm/hr	millimeters per hour
MRMS	Multi-Radar/Multi-Sensor
MSE	mean square error
MT	model tree
MTG	Model Tree Generator
MTG(2)	MTG with sum squared residuals using multiple linear regression with quantile sampling
NARR	North American Regional Reanalysis
NASA	National Aeronautics and Space Administration
NOAA	National Oceanic and Atmospheric Administration
NSE	Nash-Sutcliff model efficiency coefficient
OV_ ROUGH2D	roughness coefficients for overland flow
PCNN	precipitation estimation from CNN
PCCSCDR	PERSIANN-Cloud Classification System-Climate Data Record
PDIR-Now	PERSIANN Dynamic Infrared-Rain Rate Model
PERSIANN	Precipitation Estimation from Remotely Sensed Information using Artificial Neural Networks
PNARR	precipitation estimation from the North American Regional Reanalysis
POD	probability of detection
r	The Pearson correlation coefficient that quantifies the linear correlation
rBIAS	relative bias
REFDK	hydraulic conductivity
REFKDT	infiltration coefficient
RETDEPRTFAC	scaling factor for maximum retention depth
RF	random forest
RMSE	root mean square error
RNN	recurrent neural network
ROC	relative operating characteristics
RR	rain rate

Term	Definition
S2S	Sub-seasonal-to-Seasonal
SC-DE	shuffle complex-differential evolution
SC-SAHEL	Shuffled Complex-Self Adaptive Hybrid EvoLution
SDAE	Stacked Denoising Autoencoder
SLOPE	linear groundwater basin coefficient
SMA	Simple model average
SOFM	Self-organizing feature map
SP-UCI	shuffled complex strategy with principal component analysis, developed at University of California, Irvine
SSRM	sum squared residuals with respect to the mean
SSRML	sum squared residuals using multiple linear regression
ST2	stage two
ST4	stage 4
Tb	cloud-top temperatures
TRMM	tropical rainfall measuring mission
UTC	Coordinated Universal Time
WRF-Hydro	Weather Research and Forecasting Model Hydrological modelling system
WV	Water vapor
WY	Water year

References

Afzali Gorooh, Vesta, Subodh Kalia, Phu Nguyen Kuo-lin Hsu, Soroosh Sorooshian, and Sangram Ganguly, and Ramakrishna R. Nemani. 2020. "Deep Neural Network Cloud-Type Classification (DeepCTC) Model and Its Application in Evaluating PERSIANN-CCS." *Remote Sensing,* 12(2)2. Available online: https://doi.org/10.3390/rs12020316

AghaKouchak, A., Ali Behrangi, Soroosh Sorooshian, Kuolin Hsu, Eyal Amitai. 2011. "Evaluation of Satellite-Retrieved extreme precipitation rates across the central United States." *Journal of Geophysical Research: Atmospheres*, 116(D). Available online: http://dx.doi.org/10.1029/2010JD014741

Akbari Asanjan, Ata, Tiantian Yang, Kuolin Hsu, and Soroosh Sorooshian, Junqiang Lin, Qidong Peng. 2018. "Short-Term Precipitation Forecast Based on the PERSIANN System and LSTM Recurrent Neural Networks." *Journal of Geophysical Research: Atmospheres*, 123(22) 12,543-12,563. Available online: https://doi.org/10.1029/2018JD028375

Arnault, Joel and Sven Wagner, Thomas Rummler, Benjamin Fersch, Jan Bliefernicht, Sabine Andresen, Harald Kunstmann. 2016. "Role of Runoff-Infiltration Partitioning and Resolved Overland Flow on Land-Atmosphere Feedbacks: A Case Study with the WRF-Hydro Coupled Modeling System for West Africa." *Journal of Hydrometeorology*, 17(15). Available online: https://doi.org/10.1175/JHM-D-15-0089.1

Ashouri, Hamed and Kuo-Lin Hsu, Soroosh Sorooshian, Dan K Braithwaite, Kenneth R Knapp, L. Dewayne Cecil, Brian R. Nelson, Olivier P. Prat. 2015. "PERSIANN-CDR: Daily Precipitation Climate Data Record from Multisatellite Observations for Hydrological and Climate Studies." *Bulletin of the American Meteorological Society*, 69-83. Available online: https://doi.org/10.1175/BAMS-D-13-00068.1

Behrangi, Ali and Kuo-lin Hsu, Bisher Imam, Soroosh Sorooshian, George J. Huffman, Robert J. Kuligowski. 2009. "PERSIANN-MSA: A precipitation estimation method from satellite-based multispectral analysis." *Journal of hydrometeorology*, 1414-1429. Available online: https://doi.org/10.1175/2009JHM1139.1

Di, Zhenhua, Qingyun Duan, Chen Wang, Aizhong Ye, Chiyuan Miao, Wei Gong. 2017. "Assessing the applicability of WRF optimal parameters under the different precipitation simulations in the Greater Beijing Area." *Climate dynamics*, 50, 1927-1948. Available online: https://doi.org/10.1007/s00382-017-3729-3

Faridzad, Mohammad, Tiantian Yang, Kuolin Hsu, Soroosh Sorooshian, Chan Xiao. 2018. "Rainfall frequency analysis for ungauged regions using remotely sensed precipitation information." *Journal of hydrology*, 563, 123-142. Available online: https://doi.org/10.1016/j.jhydrol.2018.05.071

Gesch, Dean B., Michael J. Oimoen, Susan Greenlee, Charles Nelson, Michael Steuck, Dean Tyler. 2002. "The national elevation data set." *Photogrammetric engineering and remote sensing* 68(1), 5-32. Available online: https://pubs.usgs.gov/publication/70156331

Gochis, D.J., M. Barlage, R. Cabell, M. Casali, A. Dugger, K. FitzGerald, M. McAllister, J. McCreight, A. RafieeiNasab, L. Read, K. Sampson, D. Yates, Y. Zhang. 2020. "The WRF-Hydro® modeling system technical description, (Version 5.1.1)." *NCAR Technical Note*, 107. Available online: https://zenodo.org/records/3625238

Gong, Wei and Qingyun Duan. 2017. "An adaptive surrogate modeling-based sampling strategy for parameter optimization and distribution estimation (ASMO-PODE)." *Environmental Modelling & Software,* 95, 61-75. Available online: https://doi.org/10.1016/j.envsoft.2017.05.005

Hayatbini, Negin, Kuo-lin Hsu, Soroosh Sorooshian, Yunji Zhang, Fuqing Zhang. 2019a. "Effective Cloud Detection and Segmentation Using a Gradient-Based Algorithm for Satellite Imagery: Application to Improve PERSIANN-CCS." *Journal of Hydrometeorology* 20(5), 901-913. Available online: https://doi.org/10.1175/JHM-D-18-0197.1

Hayatbini, Negin, Bailey Kong, Kuo-lin Hsu, Phu Nguyen, Soroosh Sorooshian, Graeme Stephens, Charless Fowlkes, Ramakrishna Nemani, Sangram Ganguly. 2019b. "Conditional Generative Adversarial Networks (cGANs) for Near Real-Time Precipitation Estimation from Multispectral GOES-16 Satellite Imageries—PERSIANN-cGAN." *Remote Sensing,* 11(19), 2193. Available online: https://doi.org/10.3390/rs11192193

Hong, Yang, Kuo-Lin Hsu, Soroosh Sorooshian, Xiaogang Gao. 2004. "Precipitation Estimation from Remotely Sensed Imagery Using an Artificial Neural Network Cloud Classification System." *Journal of Applied Meteorology*, 1834-1853. Available online: https://doi.org/10.1175/JAM2173.1

Hsu, Kou-lin, Xiaogang Gao, Soroosh Sorooshian, Hoshin V. Gupta. 1997. "Precipitation Estimation from Remotely Sensed Information Using Artificial Neural Networks." *Journal of Applied Meteorology*, 1176-1190. Available online: https://doi.org/10.1175/1520-0450(1997)036%3C1176:PEFRSI%3E2.0.CO;2

Naeini, Matin Rahnamay, Tiantian Yang, Mojtaba Sadegh, Amir AghaKouchak, Kuo-lin Hsu, Soroosh Sorooshian, Qingyun Duan, Xiaohui Lei. 2018. "Shuffled complex-self adaptive hybrid evolution (SC-SAHEL) optimization framework." *Environmental Modelling and Software,* 104, 215-235. Available online: https://doi.org/10.1016/j.envsoft.2018.03.019

Naeini, Matin Rahnamay. 2019. "Generalized Model Tree (GMT) framework for simulating rule-based hydrologic systems." *Submitted to Journal of Water Recourse Research*.

Naeini, Matin Rahnamay, Tiantian Yang, Ahmad Tavakoly, Bita Analui, Amir AghaKouchak, Kuolin Hsu, Soroosh Sorooshian. 2020. "A Model Tree Generator (MTG) Framework for Simulating Hydrologic Systems: Application to Reservoir Routing." *Water*, 12(9), 2373. Available online: https://doi.org/10.3390/w12092373

Nguyen, Phu, Soroosh Sorooshian, Andrea Thorstensen, Hoang Tran, and Phat Huynh, Thanh Pham, Hamed Ashouri, Kuolin Hsu, Amir AghaKouchak, Dan Braithwaite. 2017. "Exploring trends through 'RainSphere': research data transformed into public knowledge." *Bulletin of the American Meteorological Society*, 653-658. Available online: https://doi.org/10.1175/BAMS-D-16-0036.1

Nguyen, Phu, Eric J. Shearer, Mohammed Ombadi, Vesta A. Gorooh, Kuolin Hsu, Soroosh Sorooshian, William S. Logan, Marty Ralph. 2020. “PERSIANN Dynamic Infrared–Rain Rate Model (PDIR) for High-Resolution, Real-Time Satellite Precipitation Estimation”. *Bulletin of the American Meteorological Society,* 101, E286–E302. Available online: https://doi.org/10.1175/BAMS-D-19-0118.1

Ombadi, Mohammed and Phu Nguyen, Soroosh Sorooshian, Kuo-lin Hsu. 2018. "Developing Intensity-Duration-Frequency (IDF) Curves From Satellite-Based Precipitation: Methodology and Evaluation." *Water Resources Research*, 54(10), 7752-7766. Available online: https://doi.org/10.1029/2018WR022929

Pan, Baoxiang , Kuolin Hsu, Amir AghaKouchak, Soroosh Sorooshian, Wayne Higgins. 2019a. "Precipitation Prediction Skill for the West Coast United States: From Short to Extended Range." *Journal of Climate*, 32(1), 161-182. Available online: https://doi.org/10.1175/JCLI-D-18-0355.1

Pan, Baoxiang, Kuolin Hsu, Amir AghaKouchak, Soroosh Sorooshian. 2019b. "Improving precipitation estimation using convolutional neural network." *Water Resources Research*, 55(3), 2301-2321. Available online: https://doi.org/10.1029/2018WR024090

Qi, Youcun, Steven Martinaitis, Jian Zhang, Stephen Cocks. 2016. " A Real-Time Automated Quality Control of Hourly Rain Gauge Data Based on Multiple Sensors in MRMS System." *Journal of Hydrometeorology*, 17(6), 1675-1691. Available online: https://doi.org/10.1175/JHM-D-15-0188.1

Ralph, F.M., T. Coleman, P.J. Neiman, R.J. Zamora, M.D. Dettinger. 2013. "Observed Impacts of Duration and Seasonality of Atmospheric-River Landfalls on Soil Moisture and Runoff in Coastal Northern California ." *Journal of Hydrometeorology,* 14(2), 443-459. Available onlin: https://doi.org/10.1175/JHM-D-12-076.1

Sadeghi, Mojtaba, Ata Akbari Asanjan, Mohammad Faridzad, Phu Nguyen, Kuolin Hsu, Soroosh Sorooshian, Dan Braithwaite. 2019a ("PERSIANN-CNN: Precipitation Estimation from Remotely Sensed Information Using Artificial Neural Networks--Convolutional Neural Networks." *Journal of Hydrometeorology,* 20(12), 2273-2289. Available online: https://doi.org/10.1175/JHM-D-19-0110.1

Sadeghi, Mojtaba, Ata Akbari Asanjan, Mohammad Faridzad, Vesta Afzali Gorooh, Phu Nguyen, Kuolin Hsu, Soroosh Sorooshian, Dan Braithwaite. 2019b. "Evaluation of PERSIANN-CDR Constructed Using GPCP V2. 2 and V2. 3 and A Comparison with TRMM 3B42 V7 and CPC Unified Gauge-Based Analysis in Global Scale." *Remote Sensing,* 11(23), 2755. Available online: https://doi.org/10.3390/rs11232755

Sampson, K. and Gochis, D. 2020. "WRF Hydro GIS Pre-Processing Tools, Version 5.1.1." Boulder, CO: National Center for Atmospheric Research, Research Applications Laboratory.Available at https://github.com/NCAR/wrf_hydro_arcgis_preprocessor/releases/tag/v5.1.1

Silver, Micha, Arnon Karnieli, Hanan Ginat, E. Meiri, Erick Fredj. 2017. "An innovative method for determining hydrological calibration parameters for the WRF-Hydro model in arid regions." *Environmental Modelling & Software*, 91, 47-69. Available online: https://doi.org/10.1016/j.envsoft.2017.01.010

Sorooshian, Soroosh, Kuo-lin Hsu, Bisher Imam, Yang Hong. 2007. "Global precipitation estimation from satellite image using artificial neural networks." *Hydrological Modelling in Arid and Semi-Arid Areas*, 21-27. Cambridge University Press. Available online: http://dx.doi.org/10.1017/CBO9780511535734.003

Srivastava, Vibhava, Wendy Graham, Rafael Munoz-Carpena, Reed M. Maxwell. 2014. "Insights on geologic and vegetative controls over hydrologic behavior of a large complex basin--global sensitivity analysis of an integrated parallel hydrologic model." *Journal of Hydrology*. 519(B), 2238-2257. Available online: https://doi.org/10.1016/j.jhydrol.2014.10.020

UC Berkeley. 2020. "What Is Machine Learning (ML)?" *datascience@berkeley*, the online Master of Information and Data Science. Available online: https://ischoolonline.berkeley.edu/blog/what-is-machine-learning/. last update: Feb 2022.

Verri, Giorgia, Nadia Pinardi, David Gochis, Joseph Tribbia, Antonio Navarra, Giovannni Coppini, Tomislava Vukicevic. 2017. "A meteo-hydrological modelling system for the reconstruction of river runoff: the case of the Ofanto river catchment." *Natural Hazards and Earth System Sciences*, 17(10), 1741-1761. Available online: https://doi.org/10.5194/nhess-17-1741-2017

Vitart, Federic and Robertson, F. Vitart, C. Ardilouze, A. Bonet, A. Brookshaw, M. Chen, C. Codorean, M. Déqué, L. Ferranti, E. Fucile, M. Fuentes, H. Hendon, J. Hodgson, H.-S. Kang, A. Kumar, H. Lin, G. Li, X. Liu, P. Malguzzi, I. Mallas, M. Manoussakis, D. Mastrangelo, C. MacLachlan, P. McLean, A. Minami, R. Mladek, T. Nakazawa, S. Najm, Y. Nie, M. Rixen, A. W. Robertson, P. Ruti, C. Sun, Y. Takaya, M. Tolstykh, F. Venuti, D. Waliser, S. Woolnough, T. Wu, D.-J. Won, H. Xiao, R. Zaripov, and L. Zhang. 2017. "The Subseasonal to Seasonal Prediction (S2S) Project Database." *Bulletin of the Amererican Meteorlogical Society,* 98(1), 163-173. Available online: https://doi.org/10.1175/BAMS-D-16-0017.1

Wang, Jiali Cheng Wang, Vishwas Rao, Andrew Orr, Eugene Yan, Rao Kotamarthi. 2019. "A parallel workflow implementation for PEST version 13.6 in high-performance computing for WRF-Hydro version 5.0: a case study over the midwestern United States." *Geoscientific Model Development* 12(8), 3523-3539. Available online: https://doi.org/10.5194/gmd-12-3523-2019

WMO (World Meteorological Organization). 2018. "WWRP/WCRP Sub-seasonal to Seasonal Prediction Project (S2S)". Available online: https://library.wmo.int/viewer/68589/download?file=WWRP-2018-2.pdf&type=pdf&navigator=1

Yang, Tiantian, Ata Akabri Asanjan, Mohammad Faridzad, Negin Hayatbini, Xiaogang Gao, Soroosh Sorooshian. 2017 (December). "An enhanced artificial neural network with a shuffled complex evolutionary global optimization with principal component analysis." *Information Sciences,* 418-419, 302-316. Available online: https://doi.org/10.1016/j.ins.2017.08.003

Yang, Tiantian, Xiaomang Liu, Lingling Wang, Peng Bai, Jingjing Li. 2020. "Simulating Hydropower Discharge using Multiple Decision Tree Methods and a Dynamical Model Merging Technique." *Journal of Water Resources Planning and Management* 146(2). Available online: https://doi.org/10.1061/(ASCE)WR.1943-5452.0001146

Yucel, Ismail, Alper Onen, K.K. Yilmaz, D.J. Gochis. 2015. "Calibration and evaluation of a flood forecasting system: Utility of numerical weather prediction model, data assimilation and satellite-based rainfall." *Journal of Hydrology,* 523, 49-66. Available online: https://doi.org/10.1016/j.jhydrol.2015.01.042

Zhang, Dalin. Richard A. Anthes. 1982 "A high-resolution model of the planetary boundary layer—Sensitivity tests and comparisons with SESAME-79 data." *Journal of Applied Meteorology,* 21(11), 1594-1609. Available online: https://doi.org/10.1175/1520-0450(1982)021%3C1594:AHRMOT%3E2.0.CO;2

Zhang, Jian, Kenneth Howard, Carrie Langston, Steve Vasiloff, Brian Kaney, Ami Arthur, and Suzanne Van Cooten, Kevin Kelleher, David Kitzmiller, Feng Ding, Dong-Jun Seo, Ernie Wells, Chuck Dempsey. 2011. "National Mosaic and Multi-Sensor QPE (NMQ) system: Description, results, and future plans." *Bulletin of the American Meteorological Society* 92(10), 1321-1338. Available online: https://doi.org/10.1175/2011BAMS-D-11-00047.1

Zhang, Jian, Kenneth Howard, Carrie Langston, Brian Kaney, Youcun Qi, Lin Tang, Heather Grams, Yadong Wang, Stephen Cocks, Steven Martinaitis, Ami Arthur, Karen Cooper, Jeff Brogden, David Kitzmiller. 2016. "Multi-Radar Multi-Sensor (MRMS) Quantitative Precipitation Estimation: Initial Operating Capabilities ." *Bulletin of the American Meteorological Society*, 97(4), 621-638. Available online: https://doi.org/10.1175/BAMS-D-14-00174.1

Zhu, Hongyan, Matthew C. Wheeler, Adam H. Sobel, Debra Hudson. 2014. "Seamless precipitation prediction skill in the tropics and extratropics from a global model." *Monthly Weather Review*, 142(4), 1556-1569. Available online: https://doi.org/10.1175/MWR-D-13-00222.1

Project Deliverables

Deliverables provided by this project include:

- Project deliverables included in this final report:
  - addressing improvements to the PERSIANN Including a Module for California (draft and final)
  - Improvement of Hydrologic and Energy Demand Forecasts that Reflect Effects of Climate Change and their Application for Near Short-term Scheduling of Hydropower Operations.
- Other deliverables include benefit questionnaire and technical transfer plans.
- Additional information and data related to this research can be found at University of California, Irvine's Center for Hydrometeorology and Remote Sensing at http://chrs.web.uci.edu/resources.php.
- This project generated 13 peer-reviewed journal articles.

ENERGY RESEARCH AND DEVELOPMENT DIVISION

Appendix A: WRF Hydro Calibration Procedure

June 2024 | CEC-500-2024-059

APPENDIX A: WRF Hydro Calibration Procedure

The team used Adaptive Surrogate Modeling-based Optimization - Parameter Optimization and Distribution Estimation (ASMO-PODE) to calibrate the WRF-Hydro model. ASMO-PODE has been tested to demonstrate its utility in calibrating a land surface model (Gong and Duan, 2017) while its predecessor ASMO was successfully applied to calibrate nine parameters in the WRF model (Di et al., 2017). In this study, 160 uniform initial sampling was first conducted on the WRF-Hydro model to construct a surrogate model using Gaussian Processes Regression method. A Markov Chain Monte Carlo approach, Delayed Rejection Adaptive Metropolis (DRAM), was then used to search for the optimal parameters in the surrogate model. Based on the information obtained from the DRAM samplers, six additional model evaluations were performed and used for the construction of the surrogate model before DRAM started the next search. This process was repeated 15 times. The entire calibration consisted of 250 model runs and an optimal set of parameters with the posterior distribution was obtained.

The parameters involved in the calibration procedure are broadly the same as those used in previous studies with WRF-Hydro (Yucel et al., 2015; Silver et al., 2015; Wang et al., 2019). The global parameters include infiltration coefficient (REFKDT) and hydraulic conductivity (REFDK), which can greatly affect the amount of surface runoff, scaling factor for maximum retention depth (RETDEPRTFAC) which controls the amount of overland flow that is retained on the surface before passing to the channels and linear groundwater basin coefficient (SLOPE) which determines the deep drainage from the soil columns to the baseflow. The spatial parameters are the Manning roughness coefficients for overland flow (OV_ROUGH2D) and channel routing (MannN) and Figure A-1 shows their distribution. The parameter ranges were specified based on guidelines from the National Water Model. Where there was no information, the upper and lower bounds of the parameter range were multiplied by 1.5 and 0.5 respectively in accordance with previous studies (Zhang and Anthes, 1982; Srivastava et al., 2014). The parameters identified for calibration and results of the calibration are summarized in Table A-1 and Table A-2 respectively.

Multi-Radar/Multi-Sensor (MRMS) precipitation was used to calibrate the WRF-Hydro model and the parameters were held constant for evaluation across all precipitation products. MRMS was used as a benchmark because it incorporates rain gauge data (Figure A-2). This allows the team to focus the evaluation solely on the performance of the precipitation products without their performance being altered by the potential improvements that product-specific calibration could bring.

Figure A-1: Spatial Distribution of Manning Roughness Coefficients

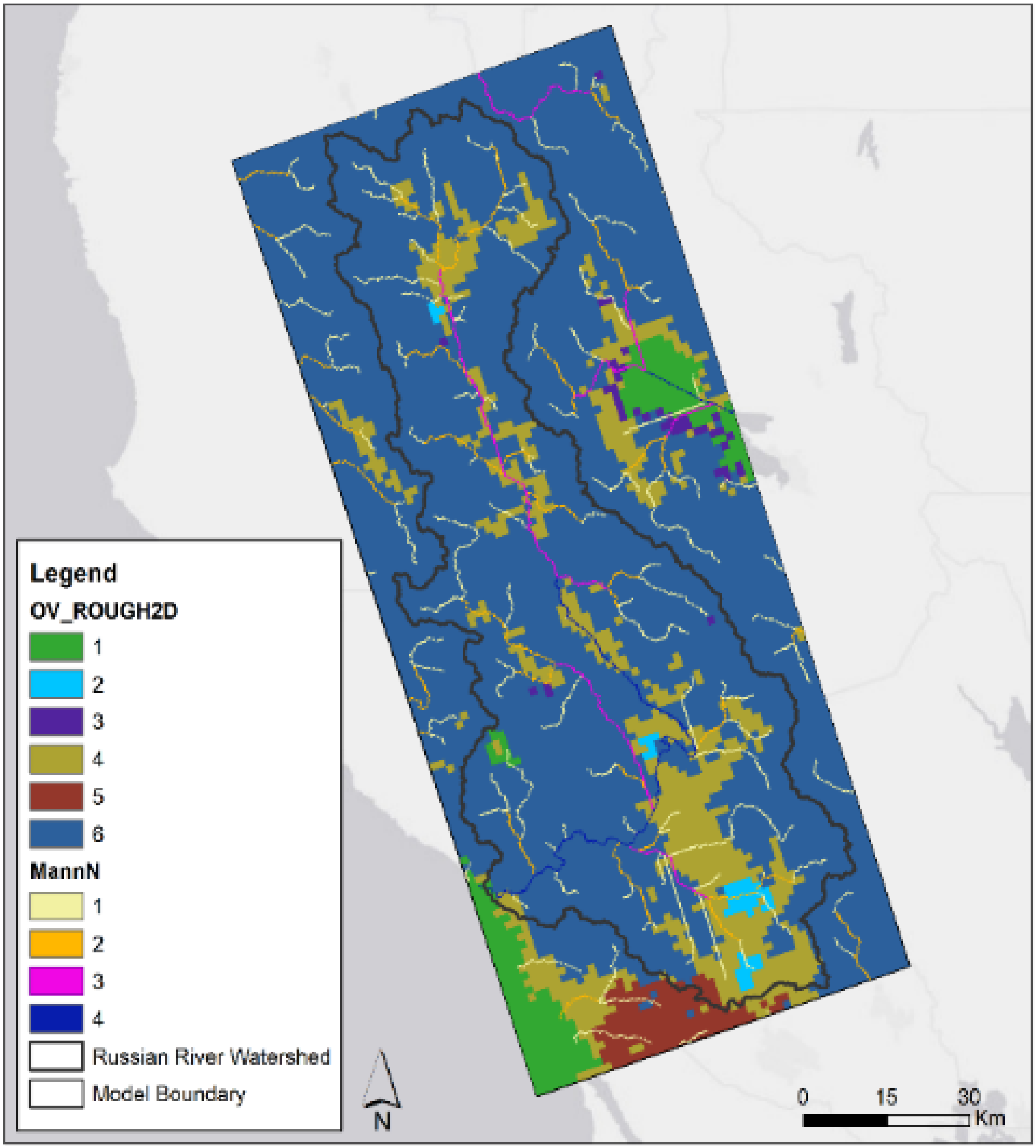

Source: Analui and Sarooshian

Table A-1: Summary of Parameters Identified for Calibration

Parameters	Description	Baseline	Lower Limit	Upper Limit
Global Parameters				
REFKDT	Infiltration partitioning parameter	3	0.0001	4.0
REFDK	Saturated hydraulic conductivity	2.0E-6	1.0E-6	3.162E-06

Parameters	Description	Baseline	Lower Limit	Upper Limit
RETDEPRTFAC	Multiplier on maximum retention depth	1.0	0.1	10.0
SLOPE	Linear groundwater basin coefficient	0.1	0.1	1.0
Distributed Parameters				
OV_ROUGH2D1	Overland flow roughness coefficient	0.005	0.0025	0.0075
OV_ROUGH2D2		0.025	0.0125	0.0375
OV_ROUGH2D3		0.035	0.0175	0.0525
OV_ROUGH2D4		0.055	0.0275	0.0825
OV_ROUGH2D5		0.0680	0.0340	0.102
OV_ROUGH2D6		0.20	0.10	0.30
MannN1	Channel routing roughness coefficient	0.55	0.275	0.825
MannN2		0.35	0.175	0.525
MannN3		0.15	0.075	0.225
MannN4		0.1	0.05	0.15

Source: Analui and Sorooshian

Table A-2: Summary of Calibrated Parameters for Each Precipitation Product

Parameters	MRMS	PERSIANN-CDR	PCCSCDR	PERSIANN-CCS	PDIR-Now
REFKDT	4.0	0.00404	0.000592	0.00136	3.025
REFDK	1.02E-06	3.126E-06	1.0E-6	3.162E-06	1.106E-06
RETDEPRTFAC	10.0	10	7.81	10	0.132
SLOPE	0.100	0.812	1.0	0.106	0.109
OV_ROUGH2D1	0.00357	0.0075	0.0075	0.0075	0.00304
OV_ROUGH2D2	0.0132	0.0263	0.0375	0.0375	0.0375
OV_ROUGH2D3	0.0263	0.0525	0.0525	0.0525	0.0353
OV_ROUGH2D4	0.0312	0.0825	0.0291	0.0340	0.0373
OV_ROUGH2D5	0.04586	0.102	0.102	0.0454	0.0460
OV_ROUGH2D6	0.11	0.296	0.290	0.30	0.106
MannN1	0.821	0.825	0.825	0.825	0.825
MannN2	0.525	0.525	0.521	0.525	0.183
MannN3	0.0917	0.225	0.223	0.225	0.225
MannN4	0.132	0.146	0.15	0.15	0.134

Source: Analuia and Soroosh Sorooshian

Figure A-2: Streamflow Simulation from WRF-Hydro Calibrated with MRMS Precipitation

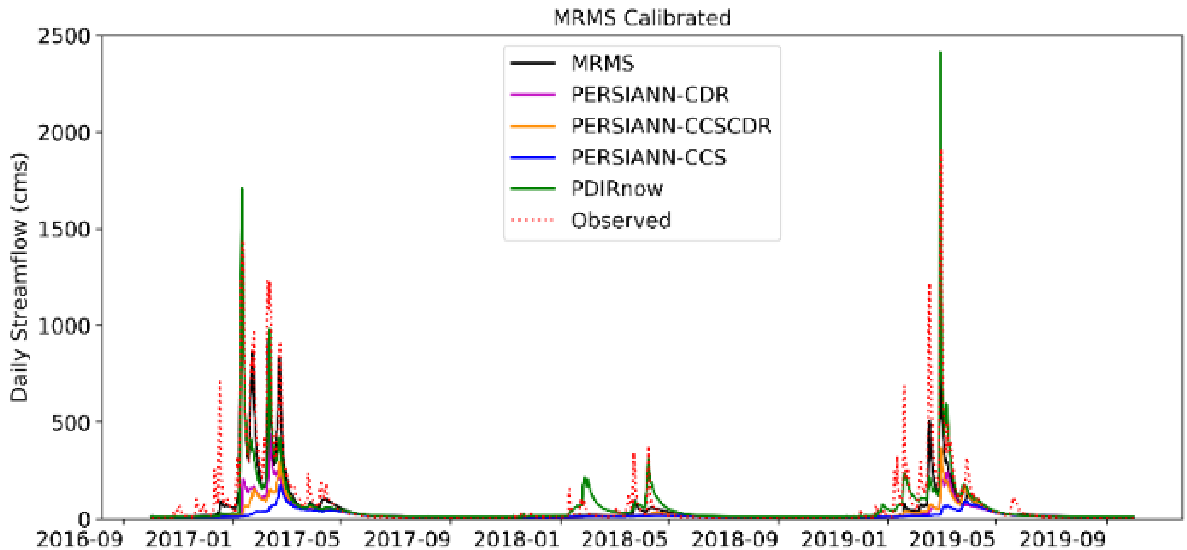

Time series comparison of the MRMS-calibrated model simulations with observed daily streamflow

Source: Analui and Sorooshian

Figure A-3 presents a time series comparison of the MRMS-calibrated model simulations with observed daily streamflow. For the calibration period from Water Year (WY) 2017 to WY 2018, there was a general agreement between the MRMS-simulated streamflow and the observed daily streamflow but there was an underestimation of the peak in May 2018. The Precipitation Estimation from Remotely Sensed Information Using Artificial Neural Networks (PERSIANN)-Cloud Classification System-Climate Data Record (PCCSCDR), PERSIANN-CDR and PERSIANN-CCS resulted in a consistent underestimation of the streamflow. PERSIANN dynamic infrared-rain rate model (PDIR-Now) was able to capture the peaks in general and performed better than MRMS for the event in May 2018. However, it overestimated the highest peak streamflow in February 2017.

For the validation period in WY 2019, the same behavior was observed as the calibration period, and this was also reflected in the statistics shown in Table A-3. All the simulations failed to hit several of the peak streamflows, indicating the limitations of the model and rainfall products in capturing such events. PDIR-Now was the closest in capturing the peak streamflows but also overestimated the highest peak streamflow in April 2019. Statistically, the MRMS derived streamflow achieved a Nash-Sutcliffe efficiency (NSE) of 0.64 root mean square error (RMSE) of 119.70 cubic meters per second and correlation coefficient of 0.93 but exhibited a substantial relative bias (rBIAS) of -43 percent. PDIR-Now showed the best performance among the satellite rainfall inputs and even outperformed MRMS slightly in NSE (0.68), RMSE (114.01) and rBIAS (-21 percent) but recorded a lower correlation of 0.83. For the other PERSIANN products, the simulations based on PERSIANN-Cloud Classification System-Climate Data Record (PCCSCDR) and PERSIANN-climate data record (CDR) were the closest and performed better than that of PERSIANN-CCS. There was a substantial negative bias for PCCSCDR, PERSIANN-CDR and PERSIANN-CCS at -61 percent, -67 percent, and -75 percent respectively. This can be attributed to the inherent underestimation in the respective precipitation data. PCCSCDR and PERSIANN-CDR showed positive NSE values of 0.20 and 0.12 respectively, indicating skills in the simulations, while PERSIANN-CCS yielded an unsatisfactory negative NSE value of -0.06. With the exception of PERSIANN-CCS which did not show good correlation with the observed streamflow (correlation coefficient 0.32), PCCSCDR and PERSIANN-CDR generally reproduced the variability of the observed streamflow (correlation coefficient 0.71 and 0.62, respectively).

Figure A-3: Scatter Plots of Simulated Streamflow Against Observed Streamflow for the Precipitation Products

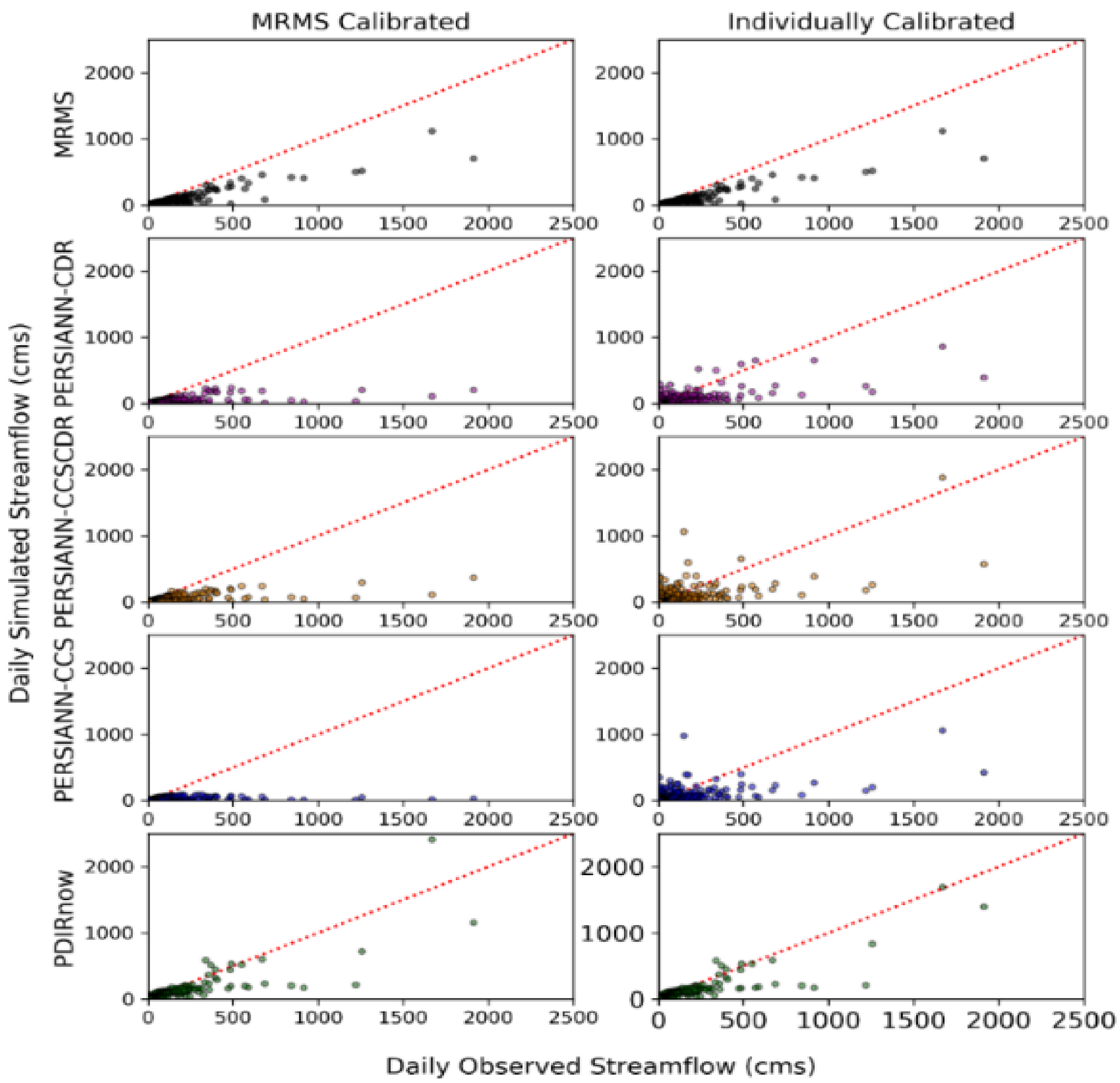

Source: Analui and Sarooshian

Table A-3: Summary Statistic of Simulated Streamflow for Validation Period

Products	NSE	CORR	RMSE	rBias
MRMS (MRMS)	0.64	0.93	119.70	-43%
PERSIANN-CDR (MRMS)	0.12	0.62	188.38	-67%
PERSIANN-CDR (Input Specific)	0.40	0.69	155.10	-40%
PCCSCDR (MRMS)	0.20	0.71	179.54	-61%
PCCSCDR (Input Specific)	0.36	0.61	160.92	-20%
PERSIANN-CCS (MRMS)	-0.06	0.32	206.35	-75%
PERSIANN-CCS (Input Specific)	0.31	0.58	167.17	-32%
PDIR-Now (MRMS)	0.68	0.83	114.01	-21%
PDIR-Now (Input Specific)	0.74	0.88	102.35	-22%

Source Analui and Sarooshian